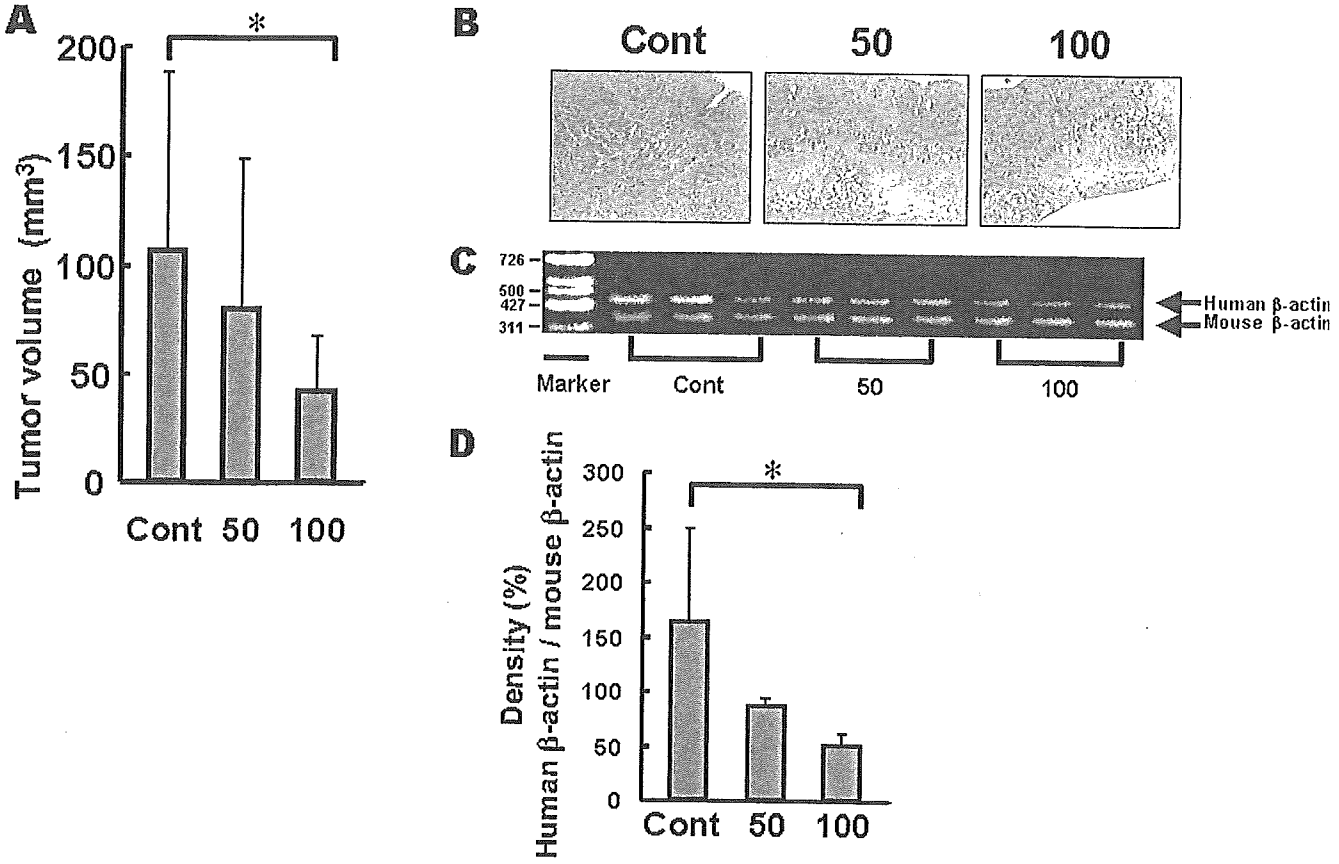

FIGURE 2 – Antitumor effect of ZD6474 in an orthotopic dissemination model *in vivo*. (*a*) *In vivo* growth-inhibitory effect of ZD6474. The implanted tumor volume was calculated after 14 days of treatment (p.o.). *Athymic mice ($n = 7$) per group were implanted with 58As1 cells, and a significant growth inhibitory effect was observed in the 100 mg/kg/day group, compared to the vehicle control group ($p = 0.027$). (*b*) Representative HE staining of tumor tissue in mice treated with ZD6474. The number of cancer cells in the sub-mucosal lesions was clearly lower and necrotic tissue was visible in the ZD6474 group, compared to the control group. (*c*) Disseminated cancer cells were collected from intraperitoneal lavage fluid to measure the ratio of tumor-derived human β-actin to murine β-actin using RT-PCR and specific primers (3 mice/group). Total RNA was equalized to 5 μg for each sample. (*d*) Densitometric analysis. Ratio of β-actin levels. *Significantly lower level of human-derived β-actin was detected in the 100 mg/kg/day ZD6474 group than in the control group ($p = 0.049$). The data shown are means ± SD. Cont, vehicle control; 50, ZD6474 50 mg/kg/day group; 100, ZD6474 100 mg/kg/day group. Significance was analyzed by Student's *t*-test.

vide particularly effective therapy for the subset of lung cancer patients whose tumor cell growth is highly dependent on EGFR signaling, including patients with tumor cells harboring activated, mutated EGFR. The proportion of patients with tumors highly dependent on EGFR signaling may be relatively small among various cancer patient populations. Therefore, additional treatment options for patients with cancers less dependent on EGFR signaling are also needed. It was concluded that 58As1 cells expressing wild-type EGFR are not highly dependent on EGFR signaling *in vitro* because the IC_{50} for growth inhibition by ZD6474 (5.8 μM) fell within the range of sensitivity reported by others for tumor cells *in vitro* (2.7–13.5 μM)[10] and because the IC_{50} for growth inhibition by gefitinib, a highly selective EGFR tyrosine kinase inhibitor, was >10μM. As a result, the concentration of ZD6474 required to inhibit 58As1 cell growth *in vitro* was 97-fold greater than required to inhibit VEGF-dependent HUVEC proliferation.[10] Nonetheless, ZD6474 significantly inhibited 58As1 tumor growth *in vivo* (Fig. 2*a*), suggesting that ZD6474 is active against gastric cancers expressing wild-type EGFR *in vivo* and that ZD6474 inhibition of tumor angiogenesis is likely to contribute significantly to this antitumor effect.

Our present study is unique because our aggressive and spontaneous intraperitoneal-dissemination model is considered a very good model of tumor progression in gastric cancer patients clinically, especially of the undifferentiated-type. Indeed, Paclitaxel and CPT-11 have been demonstrated to exhibit a growth-inhibitory effect and survival benefit in this model,[17] but gefitinib did not in preliminary result (data not shown). The positive results with ZD6474 in our present study suggest that this agent may be clinically useful in gastric cancer. We had hypothesized that direct intraperitoneal injection of ZD6474 is more effective than oral administration to inhibit intraperitoneal dissemination and result in better survival, however, the result showed that oral administration led to better survival in 44As3-inplanted mice (Fig. 3*b*).

ZD6474 inhibited the intraperitoneal dissemination of gastric cancer cells in our dissemination model. Although the mechanisms underlying this effect remain unclear, a few possibilities can be speculated: based on clinical evidence, the depth of tumor invasion and clinical staging is thought to be closely related to peritoneal dissemination.[21] Thus, one possible mechanism of the reduction of intraperitoneal dissemination may have resulted from a reduction in the serosal penetration of the cancer cells by "antitumor effect of ZD6474" on the implanted tumors. Although it is unclear whether ZD6474 has an inhibitory effect against distal metastasis to the liver and lymph nodes, for examples, it is not surprising that ZD6474 inhibits "intraperitoneal dissemination." Evaluation of its effect on distal metastasis will be the subject of a future investigation in our laboratory. Small tumor lesions (up to 2 mm) may obtain the oxygen and nutrients

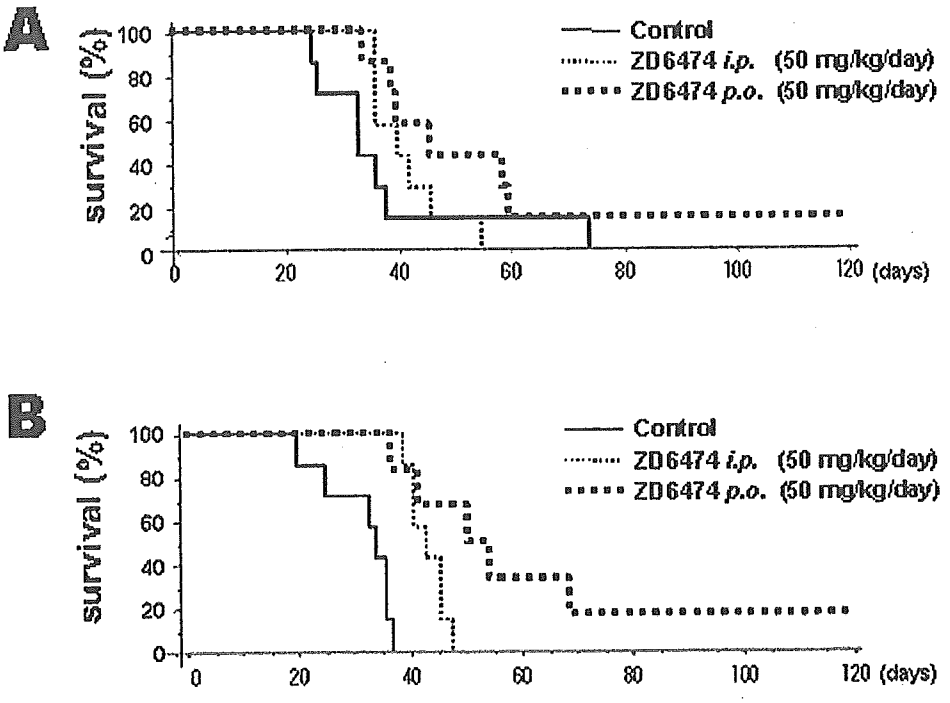

FIGURE 3 – Survival curve of 58As1 cells- (*a*) and 44As3 cells- (*b*) implanted mice treated with ZD6474. Both p.o. and i.p. administration of ZD6474 50 mg/kg/day significantly improved the survival of 44As3-implanted mice ($p = 0.0009$, $p = 0004$ *vs.* control), but did not significantly improve the survival of mice implanted with 58As1 cells ($p = 0.09$, $p = 0,4$ *vs.* control). The p values were calculated by the log-rank test.

A

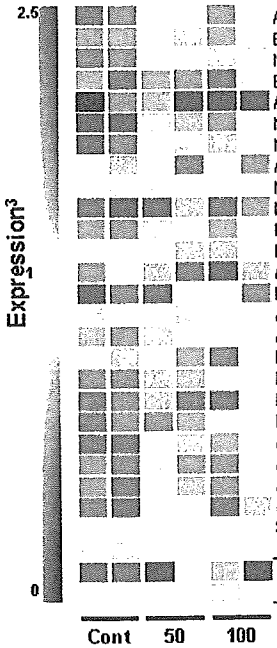

GenBank acc.no.	Gene symbol	Fold change	No. of passed[1]	Ref no.[2]
AK027138	FAM13A1	2.3	2	
BF340228	IGFBP3	2.0	2	26
NM_006931	SLC2A3	2.2	2	
BG292233	INSIG1	2.1	2	
AA654415	EST	2.8	1	
NM_001124	ADM	2.7	1	29
NM_016109	ANGPTL4	2.6	1	30
AF009664	EST	2.4	1	
NM_000935	PLOD2	2.4	1	31
NM_000596	IGFBP1	2.3	1	
BC002649	HIST1H1C	2.3	1	
NM_004929	CALB1	2.3	1	
AL110191	DSIPI	2.2	1	32
NM_006096	NDRG1	2.2	1	33
AI694562	COL4A3	2.2	1	
AL080184	INSIG2	2.1	1	
NM_002456	MUC1	2.1	1	
NM_001975	ENO2	2.1	1	34
NM_004417	DUSP1	2.0	1	
NM_013332	HIG2	2.0	1	35, 36
AL110298	SLC2A14	2.0	1	
AL132665	BNIP3L	2.0	1	37, 38
AA524505	JMJD1	2.0	1	
AA678241	SCD	2.0	1	
S81916	PGK1	2.0	1	
NM_015393	DKFZP564O0823	2.0	1	
AF257099	PTMA	0.4	1	
NM_002439	MSH3	0.4	1	

B

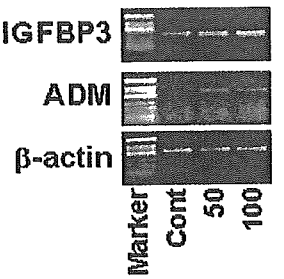

FIGURE 4 – Candidate genes for biomarkers regulated by ZD6474 treatment. Each colored block represents the expression level of a given gene in an individual sample. (*a*) Upregulated genes with a >2-fold change or <0.5-fold change are shown (mean value in the ZD6474 group/vehicle control group). Cont, vehicle control group, $n = 2$; 50, ZD6474 50 mg/kg/day group, $n = 2$; 100, ZD6474 100 mg/kg/day group, $n = 2$. [1]Number of different probes that passed fold-change criteria above. [2]Reference number for genes whose expression has been reported to be related to hypoxia. [3]Red represents increased expression and blue represents decreased expression relative to the normalized expression of the gene across all samples. (*b*) mRNA expression levels of 2 representative genes, *IGFBP-3* and *ADM*, detected by RT-PCR in tumors treated with ZD6474. *IGFBP-3* and *ADM* mRNA expression was induced in response to ZD6474.

they need by passive diffusion, but angiogenesis is required for the growth of tumors larger than 2 mm.[22] A second possible mechanism is that ZD6474 may inhibit the growth or migration of tumor vascular endothelial cells in "small tumor lesions" by inhibiting VEGFR2-dependent intracellular signaling. This effect would be expected to limit metastatic tumor growth due to lack of oxygen and nutrients, and reduce the dissemination of cancer cells.

To identify putative biomarkers of the pharmacodynamic effects of ZD6474 *in vivo*, we identified 28 candidate genes from implanted 58As1 tumor samples by oligonucleotide microarray analysis (Fig. 4*a*). IGFBP-3 has multiple functions, including in the induction of apoptosis,[23] the inhibition of cancer cell proliferation,[24] and carcinogenesis[25] and IGFBP-3 expression is transcriptionally upregulated under hypoxic conditions.[26] A recent study has also shown that EGFR regulates IGFBP-3 expression and secretion.[27] The inhibitory effect of ZD6474 on EGFR kinase may be associated with the upregulation of IGFBP-3. ADM, which was first identified in a human pheochromocytoma, is known to regulate circulation by acting as a hormone.[28] Adrenomedullin is also induced by hypoxia and may have a role in protecting against hypoxic cellular damage in human retinal pigment epithelial cells.[29] Expressions of nine of the upregulated genes, *IGFBP-3*, *ADM*, *ANGPTL4*, *PLOD2*, *DSIPI*, *NDRG1*, *ENO2*, *HIG2* and *BNIP3L*, has been reported previously to be induced by hypoxia.[26,29–38] We hypothesize that ZD6474 inhibits neovascularization in tumors, thereby limiting the oxygen and nutrient supply and resulting in tumor hypoxia and upregulation of hypoxia-inducible genes. If this hypothesis is correct, hypoxia-regulated genes and gene products might be useful biomarkers for the pharmacodynamic effects of ZD6474 and other anti-angiogenic agents in preclinical and clinical settings. We are now investigating whether these genes and gene products can be used as biomarkers for the efficacy of ZD6474 in a correlative study.

Future directions of our study include: (*i*) to compare the antitumor effect of other "anti-vascular agents" with ZD6474 in this model; (*ii*) to evaluate combination therapy with ZD6474 plus anticancer agents; (*iii*) to evaluate the antitumor effect of ZD6474 against micro-metastasis *in vivo*; and (*iv*) to confirm the usefulness of the 9 candidate genes as biomarkers in clinically.

In conclusion, we demonstrated that ZD6474 inhibited tumor growth, suppressed intraperitoneal dissemination, and prolonged survival in a highly metastatic orthotopic gastric cancer model. We carried out a microarray analysis of tumor samples and we identified 9 hypoxia-inducible genes as candidate biomarkers for monitoring the effects of ZD6474 therapy. These findings provide a strong preclinical rationale for investigating ZD6474 for the treatment of gastric cancer in the clinic.

Acknowledgements

Grants were received from the 3rd-Term Comprehensive 10-Year Strategy for Cancer Control and from a Grant-in-Aid for Scientific Research from the Ministry of Education, Culture, Sports, Science and Technology of Japan (Grant number: 12217165). T.A. is the Recipient of a Research Resident Fellowship from the Foundation of Promotion of Cancer Research in Japan.

References

1. Vanhoefer U, Rougier P, Wilke H, Ducreux MP, Lacave AJ, Van Cutsem E, Planker M, Santos JG, Piedbois P, Paillot B, Bodenstein H, Schmoll HJ, et al. Final results of a randomized phase III trial of sequential high-dose methotrexate, fluorouracil, and doxorubicin versus etoposide, leucovorin, and fluorouracil versus infusional fluorouracil and cisplatin in advanced gastric cancer: A trial of the European Organization for Research and Treatment of Cancer Gastrointestinal Tract Cancer Cooperative Group. J Clin Oncol 2000;18:2648–57.
2. Ohtsu A, Shimada Y, Shirao K, Boku N, Hyodo I, Saito H, Yamamichi N, Miyata Y, Ikeda N, Yamamoto S, Fukuda H, Yoshida S. Randomized phase III trial of fluorouracil alone versus fluorouracil plus cisplatin versus uracil and tegafur plus mitomycin in patients with unresectable, advanced gastric cancer: the Japan Clinical Oncology Group Study (JCOG9205). J Clin Oncol 2003;21:54–9.
3. Moriguchi S, Kamakura T, Odaka T, Nose Y, Maehara Y, Korenaga D, Sugimachi K. Clinical features of the differentiated and undifferentiated types of advanced gastric carcinoma: univariate and multivariate analyses. J Surg Oncol 1991;48:202–6.
4. Ferrara N, Davis-Smyth T. The biology of vascular endothelial growth factor. Endocr Rev 1997;18:4–25.
5. Nicosia RF. What is the role of vascular endothelial growth factor-related molecules in tumor angiogenesis? Am J Pathol 1998;153:11–6.
6. Mustonen T, Alitalo K. Endothelial receptor tyrosine kinases involved in angiogenesis. J Cell Biol 1995;129:895–8.
7. Shibuya M. Vascular endothelial growth factor receptor-2: its unique signaling and specific ligand, VEGF-E. Cancer Sci 2003;94:751–6.
8. Manley PW, Bold G, Bruggen J, Fendrich G, Furet P, Mestan J, Schnell C, Stolz B, Meyer T, Meyhack B, Stark W, Strauss A, et al. Advances in the structural biology, design and clinical development of VEGF-R kinase inhibitors for the treatment of angiogenesis. Biochim Biophys Acta 2004;1697:17–27.
9. Hurwitz H, Fehrenbacher L, Novotny W, Cartwright T, Hainsworth J, Heim W, Berlin J, Baron A, Griffing S, Holmgren E, Ferrara N, Fyfe G, et al. Bevacizumab plus irinotecan, fluorouracil, and leucovorin for metastatic colorectal cancer. N Engl J Med 2004;350:2335–42.
10. Wedge SR, Ogilvie DJ, Dukes M, Kendrew J, Chester R, Jackson JA, Boffey SJ, Valentine PJ, Curwen JO, Musgrove HL, Graham GA, Hughes GD, et al. ZD6474 inhibits vascular endothelial growth factor signaling, angiogenesis, and tumor growth following oral administration. Cancer Res 2002;62:4645–55.
11. Ciardiello F, Caputo R, Damiano V, Troiani T, Vitagliano D, Carlomagno F, Veneziani BM, Fontanini G, Bianco AR, Tortora G. Antitumor effects of ZD6474, a small molecule vascular endothelial growth factor receptor tyrosine kinase inhibitor, with additional activity against epidermal growth factor receptor tyrosine kinase. Clin Cancer Res 2003;9:1546–56.
12. Sandstrom M, Johansson M, Andersson U, Bergh A, Bergenheim AT, Henriksson R. The tyrosine kinase inhibitor ZD6474 inhibits tumour growth in an intracerebral rat glioma model. Br J Cancer 2004;91:1174–80.
13. McCarty MF, Wey J, Stoeltzing O, Liu W, Fan F, Bucana C, Mansfield PF, Ryan AJ, Ellis LM. ZD6474, a vascular endothelial growth factor receptor tyrosine kinase inhibitor with additional activity against epidermal growth factor receptor tyrosine kinase, inhibits orthotopic growth and angiogenesis of gastric cancer. Mol Cancer Ther 2004;3:1041–8.
14. Taguchi F, Koh Y, Koizumi F, Tamura T, Saijo N, Nishio K. Anticancer effects of ZD6474, a VEGF receptor tyrosine kinase inhibitor, in gefitinib (Iressa) sensitive and resistant xenograft models. Cancer Sci 2004;95:984–9.
15. Arao T, Fukumoto F, Takeda M, Tamura T, Saijo N, Nishio K. Small in-frame deletion in the epidermal growth factor receptor as a target for ZD6474. Cancer Res 2004;64:9101–4.
16. Yanagihara K, Tanaka H, Takigahira M, Ino Y, Yamaguchi Y, Toge T, Sugano K, Hirohashi S. Establishment of two cell lines from human gastric scirrhous carcinoma that possess the potential to metastasize spontaneously in nude mice. Cancer Sci 2004;95:575–82.
17. Yanagihara K, Takigahira M, Tanaka H, Komatsu T, Fukumoto H, Koizumi F, Nishio K, Ochiya T, Ino Y, Hirohashi S. Development and biological analysis of peritoneal metastasis mouse models for human scirrhous stomach cancer. Cancer Sci 2005;6:323–32.
18. Lynch TJ, Bell DW, Sordella R, Gurubhagavatula S, Okimoto RA, Brannigan BW, Harris PL, Haserlat SM, Supko JG, Haluska FG, Louis DN, Christiani DC, et al. Activating mutations in the epidermal growth factor receptor underlying responsiveness of non-small-cell lung cancer to gefitinib. N Engl J Med 2004;350:2129–39.
19. Paez JG, Janne PA, Lee JC, Tracy S, Greulich H, Gabriel S, Herman P, Kaye FJ, Lindeman N, Boggon TJ, Naoki K, Sasaki H, et al. EGFR mutations in lung cancer: correlation with clinical response to gefitinib therapy. Science 2004;304:1497–500.
20. Pao W, Miller V, Zakowski M, Doherty J, Politi K, Sarkaria I, Singh B, Heelan R, Rusch V, Fulton L, Mardis E, Kupfer D, et al. EGF receptor gene mutations are common in lung cancers from "never smokers" and are associated with sensitivity of tumors to gefitinib and erlotinib. Proc Natl Acad Sci USA 2004;101:13306–11.
21. Yang SH, Lin JK, Lai CR, Chen CC, Li AF, Liang WY, Jiang JK. Risk factors for peritoneal dissemination of colorectal cancer. J Surg Oncol 2004;87:167–73.
22. Folkman J. What is the evidence that tumors are angiogenesis dependent? J Natl Cancer Inst 1990;82:4–6.
23. Kim HS, Ingermann AR, Tsubaki J, Twigg SM, Walker GE, Oh Y. Insulin-like growth factor-binding protein 3 induces caspase-dependent apoptosis through a death receptor-mediated pathway in MCF-7 human breast cancer cells. Cancer Res 2004;64:2229–37.
24. Kirman I, Poltoratskaia N, Sylla P, Whelan RL. Insulin-like growth factor-binding protein 3 inhibits growth of experimental colocarcinoma. Surgery 2004;136:205–9.

25. Renehan AG, Zwahlen M, Minder C, O'Dwyer ST, Shalet SM, Egger M. Insulin-like growth factor (IGF)-I, IGF binding protein-3, and cancer risk: systematic review and meta-regression analysis. Lancet 2004;363:1346–53.
26. Koong AC, Denko NC, Hudson KM, Schindler C, Swiersz L, Koch C, Evans S, Ibrahim H, Le QT, Terris DJ, Giaccia AJ. Candidate genes for the hypoxic tumor phenotype. Cancer Res 2000;60: 883–7.
27. Takaoka M, Harada H, Andl CD, Oyama K, Naomoto Y, Dempsey KL, Klein-Szanto AJ, El-Deiry WS, Grimberg A, Nakagawa H. Epidermal growth factor receptor regulates aberrant expression of insulin-like growth factor-binding protein 3. Cancer Res 2004;64:7711–23.
28. Hirata Y, Hayakawa H, Suzuki Y, Suzuki E, Ikenouchi H, Kohmoto O, Kimura K, Kitamura K, Eto T, Kangawa K. Mechanisms of adrenomedullin-induced vasodilation in the rat kidney. Hypertension 1995;25:790–5.
29. Udono T, Takahashi K, Nakayama M, Yoshinoya A, Totsune K, Murakami O, Durlu YK, Tamai M, Shibahara S. Induction of adrenomedullin by hypoxia in cultured retinal pigment epithelial cells. Invest Ophthalmol Vis Sci 2001;42:1080–6.
30. Le Jan S, Amy C, Cazes A, Monnot C, Lamande N, Favier J, Philippe J, Sibony M, Gasc JM, Corvol P, Germain S. Angiopoietin-like 4 is a proangiogenic factor produced during ischemia and in conventional renal cell carcinoma. Am J Pathol 2003;162:1521–8.
31. Hofbauer KH, Gess B, Lohaus C, Meyer HE, Katschinski D, Kurtz A. Oxygen tension regulates the expression of a group of procollagen hydroxylases. Eur J Biochem 2003;270:4515–22.
32. Khvatova EM, Samartzev VN, Zagoskin PP, Prudchenko IA, Mikhaleva II. Delta sleep inducing peptide (DSIP): effect on respiration activity in rat brain mitochondria and stress protective potency under experimental hypoxia. Peptides 2003;24:307–11.
33. Cangul H. Hypoxia upregulates the expression of the NDRG1 gene leading to its overexpression in various human cancers. BMC Genet 2004;5:27.
34. Szturmowicz M, Burakowski J, Tomkowski W, Sakowicz A, Filipecki S. Neuron-specific enolase in non-neoplastic lung diseases, a marker of hypoxemia? Int J Biol Markers 1998;13:150–3.
35. Denko N, Schindler C, Koong A, Laderoute K, Green C, Giaccia A. Epigenetic regulation of gene expression in cervical cancer cells by the tumor microenvironment. Clin Cancer Res 2000;6:480–7.
36. Kenny PA, Enver T, Ashworth A. Receptor and secreted targets of Wnt-1/beta-catenin signalling in mouse mammary epithelial cells. BMC Cancer 2005;5:3.
37. Fei P, Wang W, Kim SH, Wang S, Burns TF, Sax JK, Buzzai M, Dicker DT, McKenna WG, Bernhard EJ, El-Deiry WS. Bnip3L is induced by p53 under hypoxia, and its knockdown promotes tumor growth. Cancer Cell 2004;6:597–609.
38. Sowter HM, Ratcliffe PJ, Watson P, Greenberg AH, Harris AL. HIF-1-dependent regulation of hypoxic induction of the cell death factors BNIP3 and NIX in human tumors. Cancer Res 2001;61: 6669–73.

online data

Epolactaene binds human Hsp60 Cys^{442} resulting in the inhibition of chaperone activity

Yoko NAGUMO*, Hideaki KAKEYA*, Mitsuru SHOJI†, Yujiro HAYASHI†, Naoshi DOHMAE‡ and Hiroyuki OSADA*[1]

*Antibiotics Laboratory, Discovery Research Institute RIKEN, 2-1 Hirosawa, Wako, Saitama 351-0198, Japan, †Department of Industrial Chemistry, Faculty of Engineering, Tokyo University of Science, Kagura-zaka, Shinjuku-ku, Tokyo 162-8601, Japan, and ‡Biomolecular Characterization Team, RIKEN Discovery Research Institute, 2-1 Hirosawa, Wako, Saitama 351-0198, Japan

Epolactaene is a microbial metabolite isolated from *Penicillium* sp., from which we synthesized its derivative ETB (epolactaene tertiary butyl ester). In the present paper, we report on the identification of the binding proteins of epolactaene/ETB, and the results of our investigation into its inhibitory mechanism. Using biotin-labelled derivatives of epolactaene/ETB, human Hsp (heat-shock protein) 60 was identified as a binding protein of epolactaene/ETB *in vitro* as well as *in situ*. In addition, we found that Hsp60 pre-incubated with epolactaene/ETB lost its chaperone activity. The *in vitro* binding study showed that biotin-conjugated epolactaene/ETB covalently binds to Hsp60. In order to investigate the binding site, binding experiments with alanine mutants of Hsp60 cysteine residues were conducted. As a result, it was suggested that Cys^{442} is responsible for the covalent binding with biotin-conjugated epolactaene/ETB. Furthermore, the replacement of Hsp60 Cys^{442} with an alanine residue renders the chaperone activity resistant to ETB inhibition, while the alanine replacement of other cysteine residues do not. These results indicate that this cysteine residue is alkylated by ETB, leading to Hsp60 inactivation.

Key words: chaperone activity, citrate synthase, covalent binding, epolactaene, heat-shock protein 60 (Hsp60), malate dehydrogenase.

INTRODUCTION

Epolactaene is a microbial metabolite isolated from the fungal strain *Penicillium* sp. BM 1689-P [1]. It was originally shown to be effective in promoting neurite outgrowth and arresting the cell cycle at the G_0/G_1 phase in a human neuroblastoma cell line, SH-SY5Y [2]. A study about epolactaene on DNA polymerase inhibition has been conducted [3,4]; however, there is no direct evidence that epolactaene interacts with those proteins in the cell. Therefore we began to study epolactaene-binding proteins in order to investigate how epolactaene affects cellular proteins and their functions.

The Hsp (heat-shock protein) 60 family is known to assist correct protein folding [5]; in addition, mammalian Hsp60 seems to have several functions in the cell, including apoptosis [6–9], an immunoregulatory function [10,11] and cell spreading [12]. Despite the importance of this molecule, little research has been conducted into mammalian Hsp60 compared with members of the prokaryotic Hsp60 family, such as GroEL. Although there is approx. 50 % sequence identity between mammalian Hsp60 and GroEL [13], they are not completely similar in structure. GroEL works only in the form of a 14-mer, double ring structure [14,15]. In contrast, human mitochondrial Hsp60 has been reported to be able to assist in protein folding in the form of a 7-mer, single ring structure [16,17]. It is also notable that mitochondrial Hsp60 is functionally active only with co-chaperone Hsp10, whereas GroEL can assist protein folding with either GroES or Hsp10 [14]. Further studies are needed to gain a detailed understanding of the molecular chaperone mechanism and functions of human Hsp60. In the present paper, we demonstrate that epolactaene and its derivative ETB (epolactaene tertiary butyl ester) bind to Hsp60 and inhibit its chaperone activity.

EXPERIMENTAL

Reagents

Monoclonal anti-Hsp60 antibody was purchased from BD Biosciences (San Jose, CA, U.S.A.). ETB was synthesized as reported in our synthetic study of epolactaene [18]. Biotin-conjugated ETB (bio–ETB) was synthesized by a coupling reaction using an activated biotin reagent [19]. The structures of ETB, its analogue and bio–ETB were determined by NMR analysis and MS.

Cell lines and culture

Human neuroblastoma SH-SY5Y cells and human cervix carcinoma HeLa cells were cultured in Dulbecco's modified Eagle's medium (Sigma, St. Louis, MO, U.S.A.), supplemented with 10 % (v/v) heat-inactivated foetal calf serum (JRH Bioscience, Lenexa, KS, U.S.A.), 50 units/ml penicillin, 50 μg/ml streptomycin (Sigma) and 1 mM sodium pyruvate (Gibco, Invitrogen Corporation, Carlsbad, CA, U.S.A.) in 5 % CO_2 at 37 °C. T-lymphoma Jurkat cells were maintained in RPMI 1640 medium (Sigma) supplemented with 10 % (v/v) heat-inactivated foetal calf serum, 50 units/ml penicillin and 50 μg/ml streptomycin.

Detection of epolactaene/ETB-binding proteins

The general procedure used to prepare the cell lysates for the detection of binding proteins has been described previously [20,21]. The lysates were incubated with or without ETB as a competitor, followed by the treatment with bio–ETB. After incubation for 1 h at 4 °C, proteins associated with bio–ETB were precipitated with streptavidin–agarose (Oncogene, San Diego, CA, U.S.A.). The bound proteins were eluted with SDS/PAGE loading buffer,

Abbreviations used: CS, citrate synthase; ETB, epolactaene tertiary butyl ester; bio–ETB, biotin-conjugated ETB; i-ETB, inactive ETB analogue; bio–i-ETB, biotin-conjugated i-ETB; HRP, horseradish peroxidase; Hsp, heat-shock protein; LC, liquid chromatography; MDH, malate dehydrogenase; NEM, *N*-ethylmaleimide; SAR, structure–activity relationship.

[1] To whom correspondence should be addressed (email hisyo@riken.jp).

separated by SDS/7.5 % PAGE, and visualized by silver staining. For immunological analysis, the separated proteins were subjected to Western blot analysis.

For the *in situ* binding assay, Jurkat cells were treated with several concentrations of biotin-conjugated derivatives for 2 h. The cells were collected in lysis buffer (10 mM Tris/HCl, pH 7.6, 1 % Nonidet P40, 0.1 % sodium deoxycholate, 0.1 % SDS and 0.15 M NaCl) containing Complete protease inhibitors (Roche, Mannheim, Germany), and the supernatants were then prepared by centrifugation at 800 *g* for 5 min, followed by centrifugation at 20 000 *g* for 15 min at 4 °C. Immobilized streptavidin magnetic beads (Promega, Madison, WI, U.S.A.) were added to the lysates, and the mixtures were incubated for 3 h at 4 °C. The bound proteins were washed and eluted by SDS/PAGE loading buffer with boiling. The separated proteins were transferred and analysed by immunoblotting with the anti-Hsp60 antibody.

Construction of human mitochondrial Hsp60–His_6 expression vector

A full-length cDNA encoding the precursor form of human mitochondrial Hsp60 [22] obtained from a Jurkat cDNA library (kindly provided by Dr S. Simizu of RIKEN) was modified so as to provide a translational start codon (AUG) at 5′ to Ala^{27}, the first amino acid of the mature protein, as described previously [23]. To this was also added a C-terminal extension of eight amino acids (LEHHHHHH), the last six being a hexahistidine tag. Two PCR primers were employed: primer 1 (5′-GCCATATGGCCAAAGATGTAAAATTTGGTG-3′) introduced an NdeI site (underlined) at the initiator methionine, while primer 2 (5′-CGCCTCGAGGAACATGCCACCTCCCATAC-3′) introduced an XhoI site (underlined) upstream of the stop codon. The PCR product was cut with NdeI and XhoI, and was ligated into the expression vector pET-21b(+) (Novagen, Darmstadt, Germany) digested with the same enzymes. The DNA sequence of this novel fusion protein was confirmed, and it will be referred to throughout the present paper as Hsp60–His_6.

Purification of recombinant mitochondrial Hsp60–His_6

Escherichia coli BL21(DE3) pLysS, transformed with the vector, was grown in LB (Luria–Bertani) medium with 100 μg/ml ampicillin at 28 °C. At a D_{600} of 0.4, IPTG (isopropyl β-D-thiogalactoside) was added to 1 mM, and the cells were shaken for an additional 10 h. A soluble cell extract was prepared, and the mitochondrial Hsp60–His_6 was purified with Ni^{2+}-nitrilotriacetate–agarose (Qiagen, Hilden, Germany) and desalted with PBS by dialysis.

Mutagenesis and mutant expression

The mutageneses of Cys^{237} to Ala (for Hsp60-1), Cys^{442} to Ala (Hsp60-2) and Cys^{447} to Ala (Hsp60-3) were performed according to the method described previously [24], using a mutagenic primer for Hsp60-1 (5′-CAAAAGGTCAGAAAGCTGAGTTCCAGGATG-3′), Hsp60-2 (5′-GTTTTGGGAGGGGGCGCCGCCCTCCTTCG-3′) or Hsp60-3 (5′-GTGCCCTCCTGCGCGCCATTCCAGCCTTG-3′). The entire sequences of Hsp60-1, 2 and 3 were analysed to ensure that only the desired mutation had been introduced. The mutant Hsp60–His_6 proteins were prepared as described above.

Chaperone activity of Hsp60

The chaperone activity of human Hsp60 (Stressgen Biotechnologies Corp., Victoria, BC, Canada) was measured using porcine heart CS (citrate synthase) (Sigma) [25] and porcine heart malate dehydrogenase (MDH) (Nacalai Tesque, Kyoto, Japan) [16], as described previously. Briefly, CS was denatured at a concentration of 15 μM in a buffer containing 6 M guanidinium chloride, 100 mM Tris/HCl, pH 8, and 20 mM dithioerythritol. Reactivation was initiated by diluting the denatured CS 100-fold into a buffer containing 100 mM Tris/HCl, pH 7.6, 10 mM $MgCl_2$, 10 mM KCl and 2 mM ATP at 20 or 35 °C with or without chaperones. Detailed information on the individual experiments are given in the legend to Figure 4. Human Hsp10 was also cloned and prepared as described previously [26]. To reconstitute the chaperone complex, Hsp60 and Hsp10 were mixed and incubated in reconstitution buffer (50 mM Tris/HCl, pH 7.6, 300 mM NaCl, 20 mM KCl, 20 mM magnesium acetate and 4 mM ATP) for 90 min at 30 °C.

For the MDH refolding assays, folding reactions were performed in 0.1 M Tris/HCl, pH 7.6, 7 mM KCl, 7 mM $MgCl_2$ and 10 mM dithiothreitol (buffer A). Porcine MDH (1 μM) was denatured in 10 mM HCl at room temperature (25 °C) for 2 h and diluted 10-fold into buffer A containing chaperones (2.1 μM Hsp60 and 4.2 μM Hsp10) pre-incubated in a reconstitution buffer. After incubation at 27 °C for 5 min, folding was initiated by the addition of 2 mM ATP. For the measurement of the ETB dose–response on the inhibition of Hsp60 mutant chaperone activities, wild-type and mutant Hsp60–His_6 proteins were used.

Hsp60 binding assay

For the *in vitro* binding assay, recombinant Hsp60–His_6 was pretreated in the presence or the absence of 10 μM NEM (*N*-ethylmaleimide) as the competitor, and then treated with bio–ETB at 4 °C. The protein samples were separated by SDS/PAGE and detected by Western blotting using avidin-conjugated HRP (horseradish peroxidase) (Pierce, Rockford, IL, U.S.A.).

Proteins were purchased from Stressgen for the binding experiment of bio–ETB with human Hsp60, Hsp70 and Hsp90. A mixture of 0.7 μM Hsp60, Hsp70 and Hsp90 was incubated with 0.35 μM bio–ETB for 1 h at 4 °C, and subjected to SDS/PAGE and Western blotting analysis.

RESULTS

Epolactaene derivatives for the screening of binding proteins

To investigate how epolactaene affects cellular proteins, we began to search for epolactaene-binding proteins in a cell lysate. During the SAR (structure–activity relationship) study for epolactaene [19], we synthesized a potent derivative, ETB, and an inactive derivative, i-ETB (Figure 1). We found that ETB is as effective as epolactaene in inhibiting the growth of several human cancer cell lines. Because of the ease of synthetic preparation, we used ETB instead of epolactaene in further studies.

On the basis of observations from the SAR studies, we also prepared bio–ETB and a biotin-conjugated inactive ETB (bio–i-ETB). ETB and i-ETB are conjugated with a biotin moiety at the ester position with an alkyl chain linker (Figure 1). Bio–ETB was found to retain the ability to inhibit growth on the SH-SY5Y and Jurkat cells, whereas bio–i-ETB was as inactive as i-ETB [19].

Identification of Hsp60 as an epolactaene/ETB-binding protein *in vitro* and *in situ*

With the biotin-conjugated probes in hand, we searched for the epolactaene/ETB-binding proteins. An SH-SY5Y cell extract was incubated with several concentrations of bio–ETB, and the bound

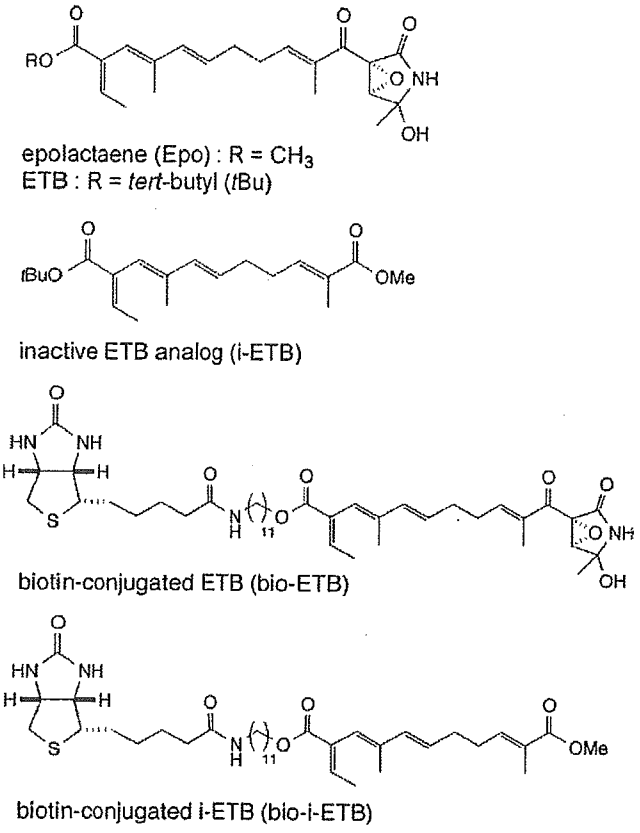

Figure 1 Chemical structures of epolactaene, ETB, i-ETB and biotin conjugates

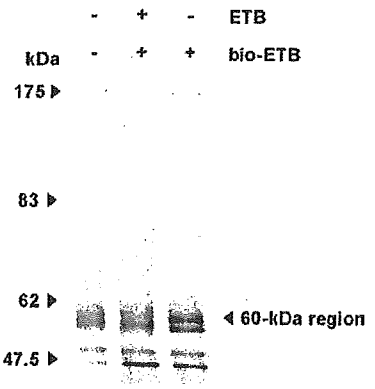

Figure 2 Screening of ETB-binding proteins

A SH-SY5Y cell lysate was pre-incubated with 70 μM ETB as a competitor, followed by treatment with 4 μM biotinylated ETB. The bound proteins were precipitated with streptavidin beads. The proteins eluted were analysed by SDS/7.5% PAGE, followed by silver staining. Molecular masses are indicated in kDa to the left of the gel.

proteins were precipitated with streptavidin beads and detected by silver staining. To minimize false positives, we used ETB as a competitor. There was a band at approx. 60 kDa, which disappeared when ETB was added as a competitor (Figure 2). Next, a large amount of eluted proteins was analysed by Coomassie Brilliant Blue staining to apply liquid chromatography (LC)–MS analysis. The 60 kDa regions were excised and digested with lysyl endopeptidase, and then the resulting peptide mixture was

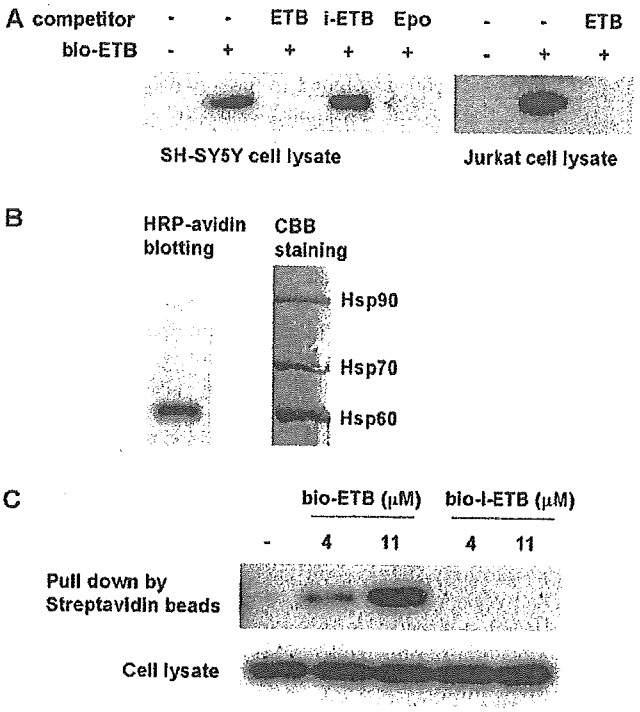

Figure 3 Identification of Hsp60 as the epolactaene/ETB-binding protein

(**A**) Immunoblot analysis of the 60 kDa protein bound to epolactaene/ETB. SH-SY5Y cell lysates were pre-incubated with 130 μM of each competitor, and the Jurkat cell lysates were pre-treated with or without 70 μM ETB, followed by 13 μM bio–ETB. The bound proteins were precipitated with streptavidin beads. These proteins were analysed by immunoblotting with the anti-Hsp60 antibody. (**B**) Binding experiment of bio–ETB with Hsp60, Hsp70 and Hsp90 *in vitro*. An equimolar mixture of human Hsp60, Hsp70 and Hsp90 was incubated with bio–ETB for 1 h at 4 °C. The proteins were separated by SDS/PAGE and analysed by HRP-conjugated avidin blotting and Coomassie Brilliant Blue (CBB) staining. (**C**) Binding of bio–ETB to Hsp60 *in situ*. Jurkat cells in culture were treated with biotin-conjugated derivatives for 2 h. The cells were collected in a lysis buffer. Immobilized streptavidin was added to the lysates, and the mixtures were incubated for 3 h at 4 °C. The bound proteins (upper panel) and whole lysates (lower panel) were analysed by immunoblotting with the anti-Hsp60 antibody.

subjected to LC–MS and MS/MS analysis. The peptide fragment from the 60 kDa band was assigned to residues 370–387 of human Hsp60 [RIQEIIEQLDVTTSEYEK, $(M + H)^+$ calculated, 2195.4; found, 2195.7]. To confirm Hsp60 as an epolactaene/ETB-binding protein, we analysed the binding protein using an anti-Hsp60 antibody (Figure 3). Western blotting experiments with the anti-Hsp60 antibody showed that Hsp60 bound to epolactaene/ETB specifically, because an excess of epolactaene/ETB blocked this association, but i-ETB did not. This association was also found in the Jurkat cell lysate, as shown in Figure 3(A). In addition, when we treated bio–ETB with an equimolar mixture of human Hsp60, Hsp70 and Hsp90 *in vitro*, Hsp60 was mainly labelled by bio–ETB (Figure 3B).

To examine whether the binding between epolactaene/ETB and Hsp60 can occur in the cells, we analysed this association *in situ* using bio–ETB derivatives. Jurkat cells were cultured with bio–ETB or bio–i-ETB for 2 h. The biotin-containing complexes were then isolated by streptavidin-immobilized beads, and the bound proteins were analysed by immunoblotting. The samples containing bio–ETB reacted with the anti-Hsp60 antibody in a concentration-dependent manner, whereas those containing bio–i-ETB showed no detectable band, demonstrating that Hsp60 bound specifically to bio–ETB (Figure 3C). These data indicate that epolactaene/ETB can bind to Hsp60 in living cells.

Inhibition by epolactaene/ETB of the chaperone activity of Hsp60

Hsp60 is a molecular chaperone which assists in protein folding. Mammalian Hsp60 was found to have two forms: cytoplasmic precursor Hsp60 and mitochondrial Hsp60. Although the two forms differ in that the former has a signal sequence in the N-terminus of the protein (1–26 amino acid residues), while the latter does not, both proteins exhibit molecular chaperone activity *in vitro* [27]. In the present study, we used recombinant human mitochondrial Hsp60 for the measurement of chaperone activity.

To determine whether epolactaene/ETB affects the chaperone activity of Hsp60, we assessed the effect of epolactaene/ETB binding on the activity of human recombinant Hsp60. CS refolding was analysed under permissive conditions (20 °C), where spontaneous reactivation could occur, or under non-permissive conditions (35 °C), where spontaneous reactivation could not occur. As shown in Figure 4(A), CS refolded to its native state in a chaperonin-independent manner under permissive conditions. ETB did not interfere with this reactivation, even at 7 μM. In contrast, the spontaneous reactivation of CS was not observed at 35 °C (Figure 4B). When either of the proteins (Hsp10 or Hsp60) was added singly, only marginal reactivation was observed. In the presence of the complete chaperonin system consisting of Hsp60 and Hsp10, a remarkable recovery of active CS was observed. When we pre-treated Hsp60 with ETB (a final concentration of 2 μM at the refolding step), the reactivation was almost completely blocked. In addition, when extra (the same amount as in the first addition) Hsp60 was added to the reaction mixture which included the ETB-pre-treated Hsp60, the reactivation was recovered, but such recovery did not occur when extra Hsp10 (the same amount as in the first addition) was added (results not shown).

In order to confirm that ETB inhibits the chaperone function of Hsp60, the other substrate, mitochondrial MDH, was used. As shown in Figure 4(C), a substantial reactivation of the denatured enzyme was observed in the presence of Hsp60 and Hsp10, although neither protein could induce reactivation when added singly. Again, when we pre-treated Hsp60 with ETB, the reactivation was blocked. The reactivation was recovered by the addition of extra Hsp60 (the same amount as in the first addition), but not by the addition of extra Hsp10 (the same amount as in the first addition) (results not shown). These results indicate that the interaction between Hsp60 and epolactaene/ETB is sufficient to affect Hsp60 chaperone activity.

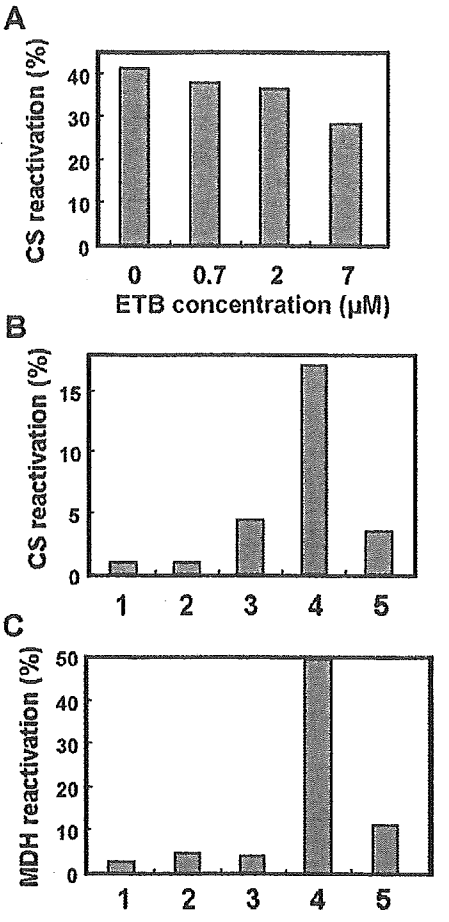

Figure 4 ETB inhibits the chaperone activity of Hsp60

The chaperone activity of Hsp60 was analysed under the following conditions. (**A**) Effects of ETB on CS reactivation at permissive conditions. Denatured CS was rapidly diluted to a concentration of 0.15 μM into a buffer (50 mM Tris/HCl, pH 7.5, 10 mM $MgCl_2$, 10 mM KCl and 15 % glycerol) with various concentrations of ETB at 20 °C. (**B**) Under non-permissive conditions, denatured CS was rapidly diluted to a concentration of 0.15 μM into a buffer (50 mM Tris/HCl, pH 7.5, 10 mM $MgCl_2$ and 10 mM KCl) containing additives (1.1 μM Hsp60 or 3.2 μM Hsp10, or both) at 35 °C. Hsp60 at 14 μM was pre-incubated with or without 2 molar equivalents of ETB in PBS at 4 °C overnight. ATP (2 mM) was added to the mixture, and after 2 h of incubation, the reactivation of CS was measured. Bar 1, no additives; bar 2, Hsp10 alone; bar 3, Hsp60 alone; bar 4, Hsp60 and Hsp10; bar 5, ETB-pre-treated Hsp60 and Hsp10. (**C**) Effects of ETB using MDH as a substrate. Denatured MDH was rapidly diluted to a concentration of 0.1 μM into a buffer (0.1 M Tris/HCl, pH 7.6, 7 mM KCl, 7 mM $MgCl_2$ and 10 mM dithiothreitol) containing additives (2.1 μM Hsp60 or 4.2 μM Hsp10, or both) at room temperature. Hsp60 was pre-treated with or without ETB, as described in (**B**). ATP (2 mM) was added to the mixture, and, after 30 min, the reactivation of MDH was measured. Bar 1, no additive; bar 2, Hsp10 alone; bar 3, Hsp60 alone; bar 4, Hsp60 and Hsp10; bar 5, ETB-pre-treated Hsp60 and Hsp10.

Cys^{442} of Hsp60 is responsible for binding with epolactaene/ETB

To determine how epolactaene/ETB modifies the function of Hsp60, we first examined the binding site of Hsp60 with epolactaene/ETB. An *in vitro* binding study (Figure 5A) demonstrated that this binding could last in the SDS/PAGE condition, because it was stained by HRP-conjugated avidin. In addition, this binding was considerably inhibited in the presence of NEM. Because NEM is a Michael acceptor, it was suggested that the covalent binding occurs in a nucleophilic manner. The α,β-unsaturated ketone, epoxide and hemi-aminal carbon of epolactaene/ETB have an electrophilic character that is potentially reactive with biological nucleophiles, such as the thiols of cysteine residues.

Human Hsp60 has three cysteine residues in the molecule. To confirm that the modification of Hsp60 function occurs as described above, the alanine mutant proteins of each of three cysteine residues (C237A, C442A and C447A) in Hsp60 were prepared in *E. coli* with a C-terminal His_6-tag. They were then tested for the ability to bind with bio–ETB. As shown in Figure 5(B), the wild-type Hsp60–His_6, C237A and C447A mutants bound with bio–ETB, but C442A lost its binding. These results suggested that Cys^{442} is responsible for covalent binding with bio–ETB.

Binding of ETB to Hsp60 via Cys^{442} is also important for the inhibition of chaperone activity by ETB

Since the activities of the cysteine mutants of human Hsp60 are not known, we first examined the ability of each mutant to facilitate productive folding. We found that the ability of these altered forms of Hsp60–His_6 to productively fold MDH was unimpaired compared with that of the wild-type Hsp60–His_6 (Figure 6, open bars).

We next investigated the ETB inhibition effects on both the wild-type and mutant Hsp60–His_6 proteins. When each protein was pre-treated with ETB, the chaperone activities of the C237A

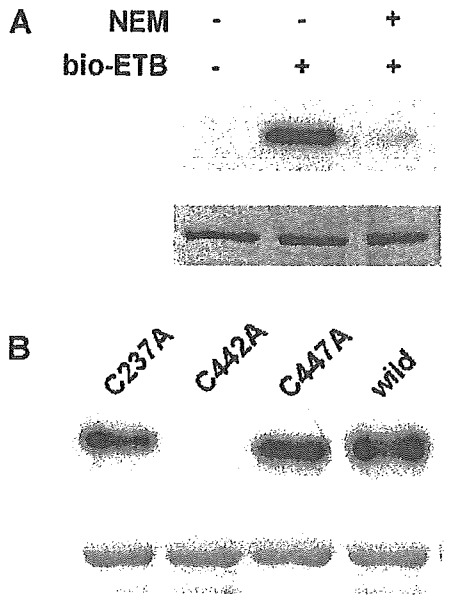

Figure 5 Cys[442] of Hsp60 is responsible for binding to epolactaene/ETB

(**A**) Competitive effect of NEM on the binding of Hsp60–His_6 to bio–ETB. Wild-type Hsp60–His_6 (1 μM) was pre-incubated with or without 10 μM NEM at 4 °C. After 4 h, 10 μM bio–ETB was added to the mixture, which was then incubated for an additional 1 h. The proteins were resolved by SDS/7.5 % PAGE and analysed by blotting with HRP-conjugated avidin (upper panel) and CBB staining (lower panel). (**B**) Binding experiments of the Hsp60 mutants with bio–ETB. The wild-type (wild) and the Hsp60–His_6 mutants (14 μM) were each incubated with 2 molar equivalents of bio–ETB at 4 °C for 12 h. Blotting with HRP-conjugated avidin (upper panel) and Coomassie Brilliant Blue staining (lower panel) were performed as described in (**A**).

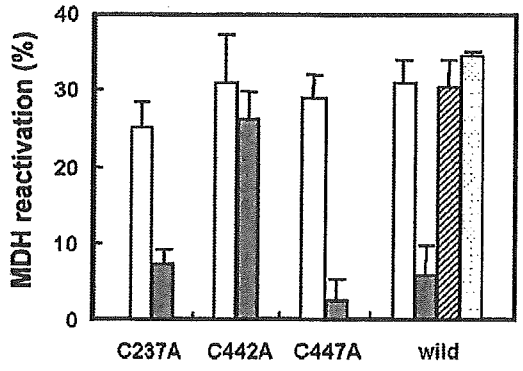

Figure 6 Inhibition by ETB of Hsp60 mutant chaperone activity on the chaperone-dependent MDH refolding

Denatured MDH was diluted 10-fold to 0.1 μM at room temperature by suspending in the buffer containing 2.1 μM each of Hsp60–His_6 mutants and 4.2 μM Hsp10–His_6 or BSA at the same protein concentration. After incubation for 5 min, ATP (2 mM, final concentration) was added to the mixture. At 30 min after the addition of ATP, an aliquot of the mixture was withdrawn, and the recovered MDH activity was measured. The reactivation by each Hsp60–His_6 mutant pre-treated with ETB (grey bars; the mutant proteins at 14 μM in PBS were incubated with 1.8 molar equivalents of ETB at 4 °C for 8 h) or without ETB (open bars) are shown. The reactivation by the wild-type (wild) Hsp60–His_6 pre-treated with 1.8 molar equivalents of NEM and 1.8 molar equivalents of mizoribine under the same conditions as ETB are shown by a hatched and a dotted bar respectively. The activity of the same amount of native MDH was taken as 100 %, and then the reactivation (%) by BSA was subtracted as the baseline. The results are the means ± S.D. for three independent experiments.

and C447A mutants, and of the wild-type Hsp60–His_6, were considerably inhibited (Figure 6, grey bars). In contrast, the chaperone activity of the C442A mutant was not abolished by ETB pre-treatment. These results indicate that the inhibition of the chaperone activity by ETB pre-treatment is derived mainly from the binding between the ETB and Cys[442] residue. In addition, these results are in agreement with the binding experiments described above (Figure 5B), which also suggested that ETB inhibits the chaperone activity by binding to Cys[442] of Hsp60.

Furthermore, we compared the inhibitory effect with NEM and mizoribine, which was reported to interfere with the chaperone activity of Hsp60 and Hsp10 at a higher concentration, 5 mM [28]. Under our experimental conditions, epolactaene/ETB inhibited Hsp60 chaperone activity at a concentration of 2–4 μM in the refolding reaction mixture. Under the same conditions as epolactaene/ETB (3.8 μM in the refolding reaction mixture), NEM and mizoribine did not show an inhibitory effect (Figure 6, hatched and dotted bars respectively).

DISCUSSION

The discovery of the binding proteins of bioactive natural compounds is one strategy for investigating their biological effects. There are many successful precedents, such as the studies on lactacystin [29], fumagillin [30], radicicol [20] and other compounds. With lactacystin, for example, the discovery that the binding target was the 20 S proteasome subunit, and that lactacystin inhibited proteasome activity [29], has promoted the exploration of not only the mode of action of lactacystin, but also the proteasome functions. In this way, the identification of binding proteins furthers biochemical research.

ETB, which is a chemically synthesized derivative of epolactaene, is as effective as epolactaene in inhibiting the growth of several human cancer cell lines [19]. Although several studies on DNA polymerase inhibition have already been conducted [3,4], the IC_{50} values of the DNA polymerase α and β inhibition by epolactaene were reported to be 25 and 100 μM respectively *in vitro*, which are considerably higher than the effective dose on the cell growth inhibition. In the present study, we searched for the binding targets of epolactaene/ETB in order to obtain direct support for the probability that epolactaene interacts with cellular proteins and disturbs its function. There were several specific or non-specific binding proteins *in vitro*, and we successfully identified human Hsp60 using bio–ETB as a bioprobe (Figures 2 and 3). The binding between Hsp60 is specific for epolactaene/ETB because the binding was blocked by the addition of epolactaene/ETB, but not by the addition of inactive analogue i-ETB. Furthermore, the finding that bio–ETB can bind Hsp60 *in situ* indicated that this complex is also formed in living cells (Figure 3C).

To elucidate the details of the interaction between ETB and Hsp60, we prepared Hsp60 mutants. Our analysis of the binding between bio–ETB and the mutant proteins suggested that Cys[442] of Hsp60 is responsible for the binding (Figure 5B). To determine how this binding affects the Hsp60 chaperone activity, we first analysed the chaperone activity of each cysteine mutant, since the mutants of human Hsp60 have scarcely been explored [16]. We found that the chaperone activity of mutant Hsp60–His_6, using MDH as a substrate, was almost the same as that of the wild-type Hsp60–His_6 (Figure 6). ETB blocked the chaperone activities of the wild-type protein and of the C237A and C447A mutant proteins, but not that of the C442A mutant (Figure 6), indicating that epolactaene/ETB binding to Cys[442] disrupts the chaperone activity. Based on sequence alignment and a comparison with the reported GroEL crystal structures [31], Cys[442] is predicted to lie near the ATP binding site (see Supplemental Figure 1 at http://www.BiochemJ.org/bj/387/bj3870835add.htm), although none of the three cysteine residues in Hsp60 is conserved in GroEL. The ATP pocket is suggested to be important not only for ATPase activity, but also for oligomerization [14,32]. Therefore interaction with

ETB may disturb the nucleotide pocket and result in the loss of ATPase activity or the destabilization of oligomeric structures, or both, although it is difficult to determine which is responsible for the inhibition.

To date, there are scarcely any natural compounds known which bind and inhibit mammalian Hsp60 chaperone activity. The 60 kDa chaperones constitute a family of proteins that play an important role in the folding of nascent, translocated and stress-denatured proteins [5]. In addition, mammalian Hsp60 has been reported to have several functions in the cell [6–12]. Using mizoribine, which inhibits the chaperone activity of mammalian Hsp60/Hsp10 at 5 mM [28], the association of Hsp60 with integrin $\alpha_3\beta_1$ was investigated [12]. Hsp60-binding compounds would be very useful for studying mammalian Hsp60 functions. In the present study, we discovered that bio–ETB covalently binds to Cys^{442} of Hsp60 and inhibits its chaperone activity. As far as we know, this is the first example of human Hsp60 covalently modified by a natural compound in a site-specific way.

In conclusion, we have demonstrated that epolactaene/ETB binds human Hsp60 *in vitro* and *in situ*, and that epolactaene/ETB inhibited the chaperone activity of human Hsp60. Furthermore, we have revealed that Cys^{442} of Hsp60 is responsible for the covalent binding of epolactaene/ETB, and have shown the resistance of the C442A mutant to ETB inhibition, suggesting this binding resulted in the inhibition of the chaperone activity. These observations of how epolactaene/ETB inhibits the chaperone activity will be helpful for gaining an understanding of the human Hsp60 multifunctions and the mechanisms of molecular chaperones.

We are grateful to K. Ishida for his helpful comments. This work was supported in part by a Grant-in-Aid from the Ministry of Education, Culture, Sports, Science and Technology of Japan, by Grant-in-Aid for Cancer Research from the Ministry of Health, Labour, and Welfare of Japan, by the Chemical Biology project (RIKEN), and by funding from the Special Postdoctoral Researchers Program (to Y. N.).

REFERENCES

1 Kakeya, H., Takahashi, I., Okada, G., Isono, K. and Osada, H. (1995) Epolactaene, a novel neuritogenic compound in human neuroblastoma cells, produced by a marine fungus. J. Antibiot. **48**, 733–735
2 Kakeya, H., Onozawa, C., Sato, M., Arai, K. and Osada, H. (1997) Neuritogenic effect of epolactaene derivatives on human neuroblastoma cells which lack high-affinity nerve growth factor receptors. J. Med. Chem. **40**, 391–394
3 Nakai, J., Kawada, K., Nagata, S., Kuramochi, K., Uchiro, H., Kobayashi, S. and Ikekita, M. (2002) A novel lipid compound, epolactaene, induces apoptosis: its action is modulated by its side chain structure. Biochim. Biophys. Acta **1581**, 1–10
4 Mizushina, Y., Kobayashi, S., Kuramochi, K., Nagata, S., Sugawara, F. and Sakaguchi, K. (2000) Epolactaene, a novel neuritogenic compound in human neuroblastoma cells, selectively inhibits the activities of mammalian DNA polymerases and human DNA topoisomerase II. Biochem. Biophys. Res. Commun. **273**, 784–788
5 Thirumalai, D. and Lorimer, G. H. (2001) Chaperonin-mediated protein folding. Annu. Rev. Biophys. Biomol. Struct. **30**, 245–269
6 Kirchhoff, S. R., Gupta, S. and Knowlton, A. A. (2002) Cytosolic heat shock protein 60, apoptosis, and myocardial injury. Circulation **105**, 2899–2904
7 Shan, Y. X., Liu, T. J., Su, H. F., Samsamshariat, A., Mestril, R. and Wang, P. H. (2003) Hsp10 and Hsp60 modulate Bcl-2 family and mitochondria apoptosis signaling induced by doxorubicin in cardiac muscle cells. J. Mol. Cell. Cardiol. **35**, 1135–1143
8 Samali, A., Cai, J., Zhivotovsky, B., Jones, D. P. and Orrenius, S. (1999) Presence of a pre-apoptotic complex of pro-caspase-3, Hsp60 and Hsp10 in the mitochondrial fraction of Jurkat cells. EMBO J. **18**, 2040–2048
9 Xanthoudakis, S., Roy, S., Rasper, D., Hennessey, T., Aubin, Y., Cassady, R., Tawa, P., Ruel, R., Rosen, A. and Nicholson, D. W. (1999) Hsp60 accelerates the maturation of pro-caspase-3 by upstream activator proteases during apoptosis. EMBO J. **18**, 2049–2056
10 Bethke, K., Staib, F., Distler, M., Schmitt, U., Jonuleit, H., Enk, A. H., Galle, P. R. and Heike, M. (2002) Different efficiency of heat shock proteins (HSP) to activate human monocytes and dendritic cells: superiority of HSP60. J. Immunol. **169**, 6141–6148
11 Kol, A., Lichtman, A. H., Finberg, R. W., Libby, P. and Kurt-Jones, E. A. (2000) Cutting edge: heat shock protein (HSP) 60 activates the innate immune response: CD14 is an essential receptor for HSP60 activation of mononuclear cells. J. Immunol. **164**, 13–17
12 Barazi, H. O., Zhou, L., Templeton, N. S., Krutzsch, H. C. and Roberts, D. D. (2002) Identification of heat shock protein 60 as a molecular mediator of $\alpha_3\beta_1$ integrin activation. Cancer Res. **62**, 1541–1548
13 Venner, T. J., Singh, B. and Gupta, R. S. (1990) Nucleotide sequences and novel structural features of human and Chinese hamster hsp60 (chaperonin) gene families. DNA Cell Biol. **9**, 545–552
14 Viitanen, P. V., Lorimer, G., Bergmeier, W., Weiss, C., Kessel, M. and Goloubinoff, P. (1998) Purification of mammalian mitochondrial chaperonin 60 through *in vitro* reconstitution of active oligomers. Methods Enzymol. **290**, 203–217
15 Weissman, J. S., Rye, H. S., Fenton, W. A., Beechem, J. M. and Horwich, A. L. (1996) Characterization of the active intermediate of a GroEL-GroES-mediated protein folding reaction. Cell **84**, 481–490
16 Nielsen, K. L. and Cowan, N. J. (1998) A single ring is sufficient for productive chaperonin-mediated folding *in vivo*. Mol. Cell **2**, 93–99
17 Levy-Rimler, G., Viitanen, P., Weiss, C., Sharkia, R., Greenberg, A., Niv, A., Lustig, A., Delarea, Y. and Azem, A. (2001) The effect of nucleotides and mitochondrial chaperonin 10 on the structure and chaperone activity of mitochondrial chaperonin 60. Eur. J. Biochem. **268**, 3465–3472
18 Hayashi, Y., Kanayama, J., Yamaguchi, J. and Shoji, M. (2002) Diastereoselective total synthesis of both enantiomers of epolactaene. J. Org. Chem. **67**, 9443–9448
19 Nagumo, Y., Kakeya, H., Yamaguchi, J., Uno, T., Shoji, M., Hayashi, Y. and Osada, H. (2004) Structure–activity relationships of epolactaene derivatives: structural requirements for inhibition of Hsp60 chaperone activity. Bioorg. Med. Chem. Lett. **14**, 4425–4429
20 Ki, S. W., Ishigami, K., Kitahara, T., Kasahara, K., Yoshida, M. and Horinouchi, S. (2000) Radicicol binds and inhibits mammalian ATP citrate lyase. J. Biol. Chem. **275**, 39231–39236
21 Miyake, Y., Kakeya, H., Kataoka, T. and Osada, H. (2003) Epoxycyclohexenone inhibits Fas-mediated apoptosis by blocking activation of pro-caspase-8 in the death-inducing signaling complex. J. Biol. Chem. **278**, 11213–11220
22 Jindal, S., Dudani, A. K., Singh, B., Harley, C. B. and Gupta, R. S. (1989) Primary structure of a human mitochondrial protein homologous to the bacterial and plant chaperonins and to the 65-kilodalton mycobacterial antigen. Mol. Cell. Biol. **9**, 2279–2283
23 Viitanen, P. V., Lorimer, G. H., Seetharam, R., Gupta, R. S., Oppenheim, J., Thomas, J. O. and Cowan, N. J. (1992) Mammalian mitochondrial chaperonin 60 functions as a single toroidal ring. J. Biol. Chem. **267**, 695–698
24 Sawano, A. and Miyawaki, A. (2000) Directed evolution of green fluorescent protein by a new versatile PCR strategy for site-directed and semi-random mutagenesis. Nucleic Acids Res. **28**, E78
25 Schmidt, M., Buchner, J., Todd, M. J., Lorimer, G. H. and Viitanen, P. V. (1994) On the role of groES in the chaperonin-assisted folding reaction: three case studies. J. Biol. Chem. **269**, 10304–10311
26 Dickson, R., Larsen, B., Viitanen, P. V., Tormey, M. B., Geske, J., Strange, R. and Bemis, L. T. (1994) Cloning, expression, and purification of a functional nonacetylated mammalian mitochondrial chaperonin 10. J. Biol. Chem. **269**, 26858–26864
27 Itoh, H., Komatsuda, A., Ohtani, H., Wakui, H., Imai, H., Sawada, K., Otaka, M., Ogura, M., Suzuki, A. and Hamada, F. (2002) Mammalian HSP60 is quickly sorted into the mitochondria under conditions of dehydration. Eur. J. Biochem. **269**, 5931–5938
28 Itoh, H., Komatsuda, A., Wakui, H., Miura, A. B. and Tashima, Y. (1999) Mammalian HSP60 is a major target for an immunosuppressant mizoribine. J. Biol. Chem. **274**, 35147–35151
29 Fenteany, G., Standaert, R. F., Lane, W. S., Choi, S., Corey, E. J. and Schreiber, S. L. (1995) Inhibition of proteasome activities and subunit-specific amino-terminal threonine modification by lactacystin. Science **268**, 726–731
30 Sin, N., Meng, L., Wang, M. Q., Wen, J. J., Bornmann, W. G. and Crews, C. M. (1997) The anti-angiogenic agent fumagillin covalently binds and inhibits the methionine aminopeptidase, MetAP-2. Proc. Natl. Acad. Sci. U.S.A. **94**, 6099–6103
31 Xu, Z., Horwich, A. L. and Sigler, P. B. (1997) The crystal structure of the asymmetric GroEL-GroES-(ADP)7 chaperonin complex. Nature (London) **388**, 741–750
32 Bochkareva, E. S., Horovitz, A. and Girshovich, A. S. (1994) Direct demonstration that ATP is in contact with Cys-137 in chaperonin GroEL. J. Biol. Chem. **269**, 44–46

Received 9 August 2004/1 December 2004; accepted 16 December 2004
Published as BJ Immediate Publication 16 December 2004, DOI 10.1042/BJ20041355

Biosci. Biotechnol. Biochem., **69** (10), 1923–1928, 2005

RKTS-33, an Epoxycyclohexenone Derivative That Specifically Inhibits Fas Ligand-Dependent Apoptosis in CTL-Mediated Cytotoxicity

Tomokazu MITSUI,[1] Yasunobu MIYAKE,[1,2] Hideaki KAKEYA,[2] Yujiro HAYASHI,[3] Hiroyuki OSADA,[2] and Takao KATAOKA[1,†]

[1]*Center for Biological Resources and Informatics, Tokyo Institute of Technology, 4259 Nagatsuta-cho, Midori-ku, Yokohama 226-8501, Japan*
[2]*Antibiotics Laboratory, Discovery Research Institute, RIKEN, 2-1 Hirosawa, Wako, Saitama 351-0198, Japan*
[3]*Department of Industrial Chemistry, Faculty of Engineering, Tokyo University of Science, Kagurazaka, Shinjuku-ku, Tokyo 162-8601, Japan*

Received May 9, 2005; Accepted June 7, 2005

Cytotoxic T lymphocytes (CTLs) eliminate virus-infected cells and tumor cells by two distinct killing pathways, mediated by lytic granules containing perforin and by Fas ligand (FasL). ECH [(*2R,3R,4S*)-2,3-epoxy-4-hydroxy-5-hydroxymethyl-6-(*1E*)-propenyl-cyclohex-5-en-1-one] has been shown to inhibit FasL-dependent apoptosis or the killing pathway in short-term culture. However, since ECH exhibited cell toxicity in long-term culture, we attempted the synthesis of less toxic epoxycyclohexenone derivatives. In the present study, we found that RKTS-33 [(*2R,3R,4S*)-2,3-epoxy-4-hydroxy-5-hydroxymethyl-cyclohex-5-en-1-one] has cell toxicity lower than ECH in long-term culture, and further investigated the inhibitory effect of RKTS-33 on CTL-mediated killing pathways. RKTS-33 did not affect cell-surface expression of FasL upon CD3 stimulation, but profoundly inhibited the FasL-dependent killing pathway mediated by CD4$^+$ and CD8$^+$ CTLs, indicating that RKTS-33 specifically blocks target cell apoptosis but not CTL function. By contrast, RKTS-33 did not affect the perforin-dependent killing pathway in CD8$^+$ CTLs. These results indicate that RKTS-33 is a specific inhibitor of the FasL-dependent killing pathway in CTL-mediated cytotoxicity.

Key words: apoptosis; cytotoxic T lymphocyte (CTL); (*2R,3R,4S*)-2,3-epoxy-4-hydroxy-5-hydroxymethyl-6-(*1E*)-propenyl-cyclohex-5-en-1-one (ECH); Fas ligand; (*2R,3R,4S*)-2,3-epoxy-4-hydroxy-5-hydroxymethyl-cyclohex-5-en-1-one (RKTS-33)

Cytotoxic T lymphocytes (CTLs) induce apoptosis in target cells through two distinct killing pathways, mediated by lytic granules that contain the pore-forming protein perforin and serine proteases known as granzymes and by Fas ligand (FasL).[1,2] Upon recognition of target cells *via* T cell receptor (TCR), CTLs rapidly release lytic granules into the interface between CTLs and target cells.[1,2] Perforin facilitates translocation of granzymes A and B into the cytosol, leading to target cell apoptosis.[3] Granzyme B triggers caspase-dependent apoptosis, whereas granzyme A initiates caspase-independent apoptosis.[4,5] Upon TCR stimulation, CTLs are also induced to express FasL on the cell surface.[1,2] Ligation of Fas by FasL induces recruitment of FADD and procaspase-8, resulting in the formation of the death-inducing signaling complex (DISC).[6,7] In the DISC, procaspase-8 undergoes dimerization and subsequent self-cleavage, generating the active heterotetramer. Active caspase-8 cleaves downstream substrates such as procaspase-3 and the Bcl-2 family member Bid, leading to apoptosis execution.

Recently, we reported that an epoxycyclohexenone derivative [(*2R,3R,4S*)-2,3-epoxy-4-hydroxy-5-hydroxymethyl-6-(*1E*)-propenyle-cyclohex-5-en-1-one] (ECH; Fig. 1A) blocks activation of procaspase-8 in the DISC and thereby inhibits death receptor-mediated apoptosis, while death receptor-independent apoptosis induced by chemicals and UV irradiation is totally insensitive to ECH.[8] Consistent with these findings, we have shown that ECH inhibits FasL-dependent apoptosis of target cells induced by CD4$^+$ and CD8$^+$ CTLs, but barely influences perforin-dependent DNA fragmentation and cytolysis of target cells mediated by CD8$^+$ CTLs.[9] These findings indicate that ECH is a specific inhibitor of the FasL-dependent CTL-mediated killing pathway. However, since ECH itself exhibited cell toxicity in

† To whom correspondence should be addressed. Fax: +81-45-924-5832; E-mail: tkataoka@bio.titech.ac.jp

Abbreviations: CMA, concanamycin A; CTLs, cytotoxic T lymphocytes; DISC, death-inducing signaling complex; DTAF, dichlorotriazinylaminofluorescein; ECH, (*2R,3R,4S*)-2,3-epoxy-4-hydroxy-5-hydroxymethyl-6-(*1E*)-propenyl-cyclohex-5-en-1-one; E:T, effector:target; FasL, Fas ligand; IC_{50}, 50% inhibitory concentration; KLH, keyhole limpet hemocyanin; MTT, 3-[4,5-dimethylthiazol-2-yl]-2,5-diphenyltetrazolium bromide; RKTS-33, (*2R,3R,4S*)-2,3-epoxy-4-hydroxy-5-hydroxymethyl-cyclohex-5-en-1-one; TCR, T cell receptor; TdR, thymidine

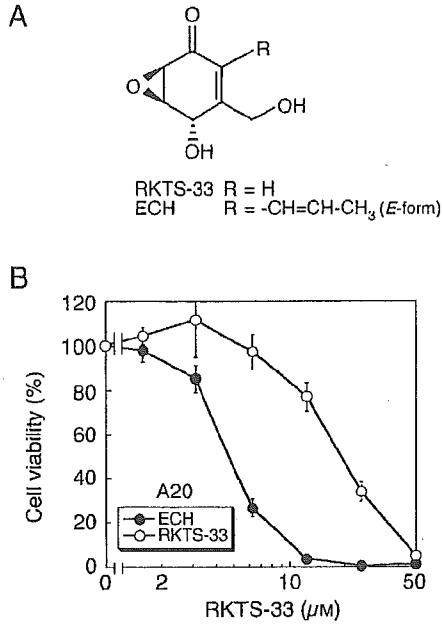

Fig. 1. RKTS-33 Has Lower Toxicity Than ECH.

A, Structures of ECH and RKTS-33. B, A20 cells were incubated with the indicated concentrations of ECH (●) or RKTS-33 (○) for 3 d. Cell viability (%) was measured by MTT assay. The data points represent the mean ± SD of triplicate cultures.

long-term culture, ECH might be applicable only to the short-term killing assay.

A series of epoxycyclohexenone derivatives were asymmetrically synthesized *via* key synthetic intermediates obtained from lipase-catalyzed kinetic resolution.[10] RKTS-33 [(*2R,3R,4S*)-2,3-epoxy-4-hydroxy-5-hydroxymethyl-cyclohex-5-en-1-one] (Fig. 1A) has been found to inhibit FasL-induced apoptosis as almost effectively as ECH without any inhibitory effect on staurosporine-induced apoptosis in human leukemia cell lines.[10] In the present study, we found that RKTS-33 has cell toxicity lower than ECH in long-term culture, and further investigated the inhibitory effect of RKTS-33 on CTL-mediated killing pathways.

Materials and Methods

Cells. CTL clones and target cells were kindly provided by Dr. N. Shinohara (Department of Immunology, Kitasato University School of Medicine, Kanagawa, Japan). The H-2^d-specific $CD8^+$ CTL clone OE4,[11] the keyhole limpet hemocyanin (KLH)-specific H-2^d (I-E^d)-restricted $CD4^+$ CTL clone BK-1,[12] mouse B lymphoma A20, A20.HL, and A20.FO derived from BALB/c mice (H-2^d), mouse thymic lymphoma L5178Y derived from DBA/2 mice (H-2^d), and the Fas-expressing transfectant of L5178Y (L5178Y-Fas)[13] were maintained as described in our previous paper.[9] A20.HL cells were BALB/c B lymphoma transfected with light and heavy chain genes of anti-trinitrophenol IgM antibody.[14] A20.FO cells were the Fas-negative variant subcloned from Fas-positive A20.2J cells.[15]

Reagents. RKTS-33 and ECH were synthesized as described previously.[10] Concanamycin A (CMA) and GM6001 were purchased from Wako Pure Chemical Industries, Ltd. (Osaka, Japan) and Calbiochem (San Diego, CA), respectively. Recombinant human soluble FasL[16] was a gift from Dr. J. Tschopp (Department of Biochemistry, University of Lausanne, Epalinges, Switzerland).

Cell viability assay. A20 cells were incubated with the indicated concentrations of RKTS-33 or ECH for 3 d and then pulsed with 500 μg/ml of 3-[4,5-dimethylthiazol-2-yl]-2,5-diphenyltetrazolium bromide (MTT) (Sigma, St. Louis, MO) for 4 h in 96-well microtiter plates. MTT-formazan was then solubilized with 5% SDS overnight, and A_{595} was measured. Cell viability (%) was calculated as (experimental A_{595} − background A_{595})/(control A_{595} − background A_{595}) × 100.

DNA fragmentation assay. Target cells were labeled with 37 kBq of [methyl-^{3}H] thymidine (TdR; ICN Biomedicals, Costa Mesa, CA) for 16 h and washed three times before use. [methyl-^{3}H]TdR-labeled cells (1×10^5 cells/ml, 100 μl) were preincubated with the indicated concentrations of RKTS-33 or ECH and mixed with equal volumes of CTL suspension in round-bottom 96-well microtiter plates, followed by centrifugation (300 × *g*, 3 min). The concentrations of RKTS-33 during 4 h coculture with CTLs was diluted to half the initial concentrations. At the end of culture, the cells were lysed by pipetting in the presence of 0.1% Triton X-100. After centrifugation (600 × *g*, 5 min), the supernatants were harvested and measured for radioactivity. Specific ^{3}H-DNA release was calculated using the following formula: (experimental cpm − spontaneous cpm)/(maximum cpm − spontaneous cpm) × 100.

Analysis of granule exocytosis. Granule exocytosis was analyzed as described in our previous paper.[9] Briefly, OE4 cells were incubated in 96-well microtiter plates coated with or without anti-mouse CD3 antibody 145-2C11. The granzyme A activity of the culture supernatants was measured using N^{α}-benzyloxycarbonyl-L-lysine thiobenzyl ester.

Analysis of FasL expression. Biotinylated anti-mouse FasL antibody FLIM58[17] was kindly provided by Dr. T. Suda (Cancer Research Institute, Kanazawa University, Kanazawa, Japan). CTL clones (1×10^6 cells) were stained with biotinylated FLIM58 for 45 min and then stained with dichlorotriazinylaminofluorescein (DTAF)-streptavidin (Jackson Immunoresearch Laboratories, West Grove, PA) for 30 min followed by FACS analysis.

Results

RKTS-33 is a less toxic epoxycyclohexenone derivative than ECH

Murine B lymphoma A20 cells were incubated with RKTS-33 or ECH for 3 d, and cell viability was measured by MTT assay (Fig. 1B). ECH decreased cell viability in a dose-dependent manner, indicating that ECH has cell toxicity in long-term culture. As a less toxic epoxycylohexenone derivative, RKTS-33 exhibited 4-fold lower cell toxicity to A20 cells than did ECH.

RKTS-33 inhibits Fas-mediated apoptosis induced by soluble FasL

A20 cells undergo DNA fragmentation upon stimulation with cross-linked FasL, whereas Fas-negative A20.FO cells are insensitive to cross-linked FasL.[9] In FasL-treated A20 cells, RKTS-33 inhibited DNA fragmentation in a dose-dependent manner, almost completely at 100 μM (Fig. 2A). Murine thymic lymphoma L5178Y-Fas cells but not L5178Y cells are sensitive to cross-linked FasL.[9] FasL-induced DNA fragmentation in L5178Y-Fas cells was prevented by RKTS-33 in a dose-dependent manner, almost completely at 100 μM (Fig. 2B).

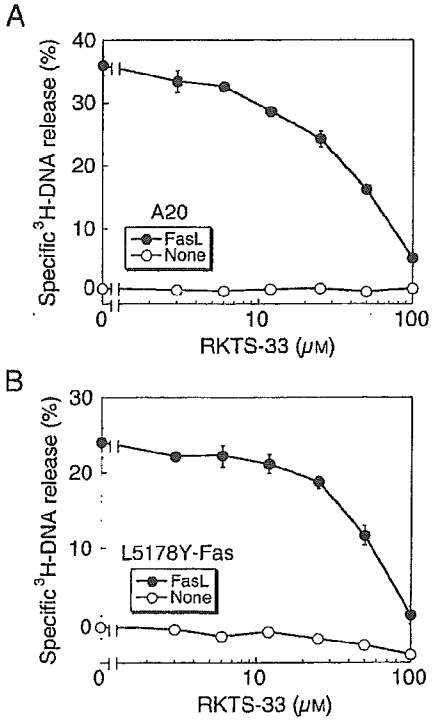

Fig. 2. RKTS-33 Inhibits DNA Fragmentation Induced by Soluble FasL.

A, [methyl-^{3}H]TdR-labeled A20 cells were preincubated with serial dilutions of RKTS-33 for 1 h and then incubated in the presence (●) or the absence (○) of cross-linked FasL for 4 h. B, [methyl-^{3}H]TdR-labeled L5178Y-Fas cells were preincubated with serial dilutions of RKTS-33 for 2 h and then incubated in the presence (●) or the absence (○) of cross-linked FasL for 4 h. The radioactivity of the fragmented DNA was measured. The data points represent the mean ± SD of triplicate cultures.

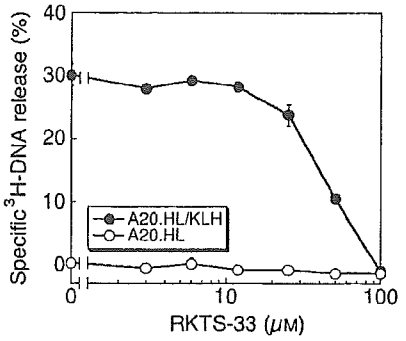

Fig. 3. RKTS-33 Inhibits the FasL-Dependent Killing Pathway Mediated by CD4$^+$ CTLs.

[methyl-^{3}H]TdR-labeled A20.HL cells were pulsed with or without KLH (300 μg/ml) prior to assay. KLH-pulsed A20.HL cells (●) and nonpulsed A20.HL cells (○) were preincubated with serial dilutions of RKTS-33 for 1 h and then cultured with BK-1 cells (E:T cell ratio = 8) for 4 h. The radioactivity of the fragmented DNA was measured. The data points represent the mean ± SD of triplicate cultures.

RKTS-33 inhibits the FasL-dependent killing pathway mediated by CD4$^+$ CTLs

The KLH-specific CD4$^+$ CTL clone BK-1 cells are perforin-negative and kill target cells *via* the FasL-dependent killing pathway.[13,18] BK-1 cells are able to induce DNA fragmentation only when A20.HL cells are pulsed with KLH. Similarly to DNA fragmentation induced by soluble FasL, RKTS-33 inhibited FasL-dependent DNA fragmentation mediated by BK-1 cells (Fig. 3).

RKTS-33 does not inhibit the perforin-dependent killing pathway mediated by CD8$^+$ CTLs

The H-2^d-specific CD8$^+$ CTL clone OE4 cells kill Fas-negative A20.FO cells and L5178Y cells only *via* the perforin-dependent killing pathway. RKTS-33 failed to affect DNA fragmentation induced by OE4 cells even when A20.FO cells and L5178Y cells were pretreated with 100 μM RKTS-33 (Fig. 4A, B).

RKTS-33 inhibits the FasL-dependent killing pathway mediated by CD8$^+$ CTLs

A20 cells and L5178Y-Fas cells express cell-surface Fas and are induced to undergo apoptosis by OE4 cells *via* both the perforin-dependent and the FasL-dependent killing pathways. Vacuolar type H$^+$-ATPase inhibitor CMA specifically blocks the perforin-dependent killing pathway.[15] Although RKTS-33 did not affect DNA fragmentation induced by OE4 cells without CMA pretreatment, FasL-dependent DNA fragmentation induced by CMA-treated OE4 cells was inhibited by RKTS-33 in a dose-dependent manner (Fig. 5A), as observed with DNA fragmentation induced by soluble FasL (Fig. 2A). In contrast to A20 cells, L5178Y-Fas

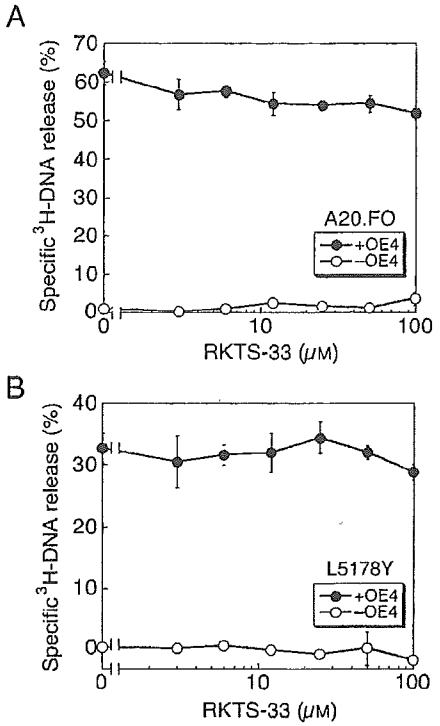

Fig. 4. RKTS-33 Does Not Affect the Perforin-Dependent Killing Pathway by CD8$^+$ CTLs.

A, [methyl-^{3}H]TdR-labeled A20.FO cells were preincubated with serial dilutions of RKTS-33 for 1 h and then cultured with (●) or without (○) OE4 cells (E:T cell ratio = 2) for 4 h. B, [methyl-^{3}H]TdR-labeled L5178Y-Fas cells were preincubated with serial dilutions of RKTS-33 for 2 h and then cultured with (●) or without (○) OE4 cells (E:T cell ratio = 2) for 4 h. The radioactivity of the fragmented DNA was measured. The data points represent the mean ± SD of triplicate cultures.

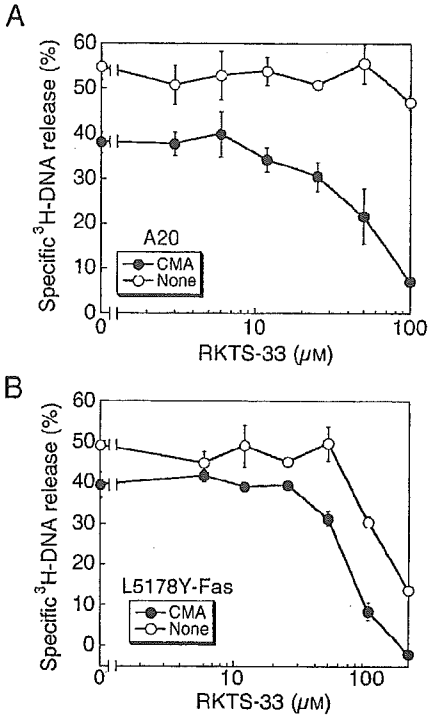

Fig. 5. RKTS-33 Inhibits the FasL-Dependent Killing Pathway Mediated by CD8$^+$ CTLs.

A, OE4 cells were preincubated with (●) or without (○) CMA (100 nM) for 2 h. [methyl-^{3}H]TdR-labeled A20 cells were preincubated with serial dilutions of RKTS-33 for 1 h and then cultured with OE4 cells (E:T cell ratio = 2) for 4 h. B, [methyl-^{3}H]TdR-labeled L5178Y-Fas cells were preincubated with serial dilutions of RKTS-33 for 2 h and then cultured with (●) or without (○) OE4 cells (E:T cell ratio = 2) for 4 h. The radioactivity of the fragmented DNA was measured. The data points represent the mean ± SD of triplicate cultures.

cells are killed dominantly *via* the FasL-dependent pathway.[9] DNA fragmentation of L5178Y-Fas cells induced by nontreated and CMA-treated OE4 cells was dose-dependently inhibited by RKTS-33 (Fig. 5B).

RKTS-33 does not affect effector/target conjugate formation

To exclude the possibility that RKTS-33 influences CTL-target interaction, RKTS-33-pretreated A20 cells were mixed with OE4 cells, and the resulting conjugate formation was analyzed. RKTS-33 did not affect conjugate formation between OE4 cells and A20 cells even when A20 cells were pretreated with RKTS-33 at 100 μM (data not shown).

RKTS-33 partially affects granule exocytosis in CD8$^+$ CTLs

OE4 cells release lytic granules into the culture medium when incubated with plate-bound anti-TCR or anti-CD3 antibody. In contrast to coculture with target cells, CD3 stimulation can induce abundant release of granzyme A. In the present experimental system, RKTS-33 partially reduced CD3-induced granule exocytosis (Fig. 6), but RKTS-33 barely affected the perforin-dependent killing pathway mediated by OE4 cells (Fig. 4). These data suggest the possibility that excess amounts of lytic granules are exocytosed from CTLs to target cells and that a portion of the granular components (perforin and granzymes) is sufficient to induce target cell apoptosis.

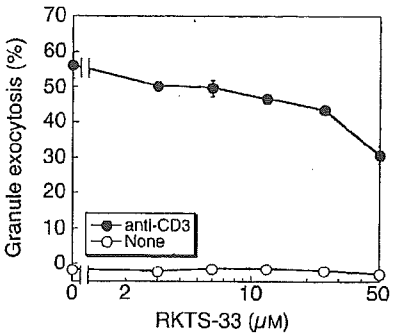

Fig. 6. Effect of RKTS-33 on Granule Exocytosis.

OE4 cells were incubated with (●) or without (○) immobilized anti-CD3 antibody in the presence of serial dilutions of RKTS-33 for 4 h. Culture supernatants were measured for granzyme A activity. The data points represent the mean ± SD of triplicate cultures.

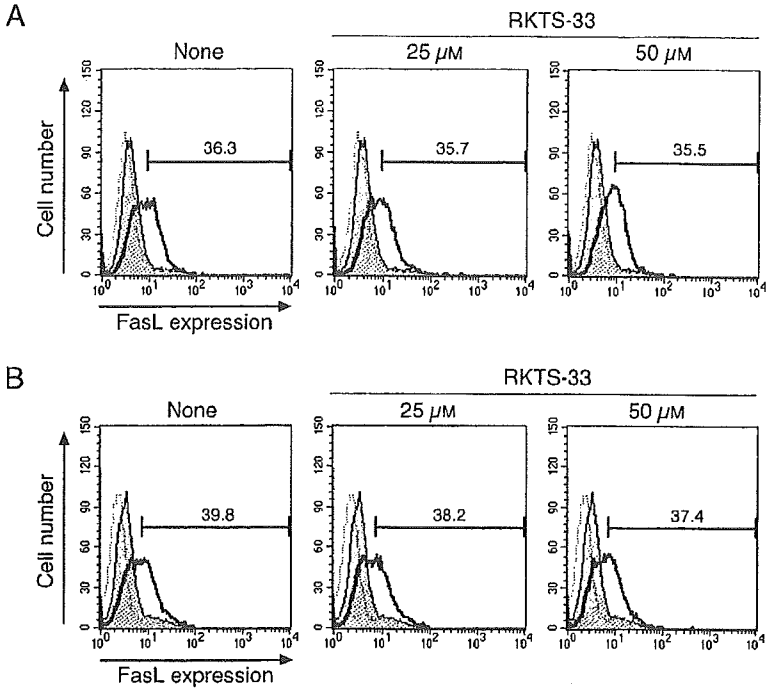

Fig. 7. Effect of RKTS-33 on Cell-Surface FasL Expression.

A and B, OE4 cells (A) and BK-1 cells (B) were incubated with (bold lines) or without (filled area) immobilized anti-CD3 antibody in the presence of GM6001 (10 μM) and the indicated concentrations of RKTS-33 for 4 h. The cells were stained with biotinylated anti-mouse FasL antibody, and then stained with DTAF-streptavidin. Dotted lines indicate unstimulated cells stained with DTAF-streptavidin alone.

RKTS-33 does not affect cell-surface FasL expression in CD4$^+$ and CD8$^+$ CTLs

TCR stimulation induces *de novo* synthesis and subsequent cell-surface expression of membrane-bound FasL. Membrane-bound FasL is converted to its soluble form by the action of metalloproteinase.[19] To investigate whether RKTS-33 inhibits cell-surface expression of FasL, OE4 cells and BK-1 cells were pretreated with RKTS-33 and stimulated with immobilized anti-CD3 antibody in the presence of the metalloproteinase inhibitor GM6001. CD3 stimulation led to strong induction of cell-surface FasL in OE4 cells and BK-1 cells, but RKTS-33 did not influence cell-surface FasL expression in these CTL clones (Fig. 7A, B). By contrast, a 30% reduction in cell-surface FasL expression was observed when OE4 cells and BK-1 cells were treated with 50 μM ECH (data not shown).

Discussion

In the present study, we found that RKTS-33 is a less toxic epoxycyclohexenone derivative than ECH in long-term culture, and further investigated the inhibitory effect of RKTS-33 on two distinct CTL-mediated killing pathways. RKTS-33 did not influence CD3-induced expression of cell-surface FasL by CD4$^+$ and CD8$^+$ CTLs, but prevented FasL-induced target cell apoptosis mediated by soluble FasL as well as CD4$^+$ and CD8$^+$ CTLs. In contrast, the perforin-dependent killing pathway mediated by CD8$^+$ CTLs was insensitive to RKTS-33. Thus our present results indicate that RKTS-33 is a specific inhibitor of the FasL-dependent killing pathway in CTL-mediated cytotoxicity.

Recently, we have shown that ECH inhibits self-activation of procaspase-8 in the DISC and specifically prevents death receptor-mediated apoptosis.[8] Furthermore, ECH inhibits the FasL-dependent killing pathway but not the perforin-dependent killing pathway in CTL-mediated cytotoxicity.[9] RKTS-33 is an ECH derivative devoid of a propenyl group at C-6.[10] RKTS-33 has been shown to inhibit FasL-dependent apoptosis but not staurosporine-induced apoptosis in human leukemia cell lines.[10] Because of the structural similarity between ECH and RKTS-33, it appears likely that RKTS-33 inhibits activation of procaspase-8 in the cell. Consistent with this, we have observed that RKTS-33 specifically inhibits the FasL-dependent killing pathway but not the perforin-dependent killing pathway in CTL-mediated cytotoxicity. Moreover, RKTS-33 did not affect expression of cell-surface FasL on CTLs, indicating that RKTS-33 specifically blocks target cell apoptosis in the CTL-mediated killing pathway.

Treatment of cultured cell lines with a general peptide-based caspase inhibitor, zVAD-fmk, efficiently blocks activation of procaspase-8 upon Fas stimulation, but does not affect their proliferative responses. The observation that ECH and RKTS-33 reduce cell viability in long-term culture suggests that these compounds have additional target molecules essential for cell cycle progression. The length of the side chain at C-6 might be important for

Table 1. Effects of RKTS-33 and ECH on CTL-Mediated Cytotoxicity

Killing pathway	Effector	Target	IC_{50} (μM) RKTS-33	ECH
Perforin	OE4	A20.FO	>100	>100
	OE4	L5178Y	>100	>100
FasL	Soluble FasL	A20	43	22
	Soluble FasL	L5178Y-Fas	49	34
	BK-1	A20.HL	50	25
	OE4 (CMA)	A20	57	27
	OE4 (CMA)	L5178Y-Fas	71	62
Perforin + FasL	OE4	A20	>100	>100
	OE4	L5178Y-Fas	128	108

binding to target molecules, since RKTS-33 is less toxic than ECH, and RKTS-35, which possesses a bulky phenyl group at C-6, shows stronger toxicity than ECH without any inhibition on Fas-dependent apoptosis.[10]

The IC_{50} values of RKTS-33 in FasL-dependent apoptosis mediated by soluble FasL and CTLs were 1.2- to 2-fold higher than those of ECH (Table 1), whereas the inhibitory concentration of RKTS-33 on the long-term proliferation of A20 cells was 4-fold higher than that of ECH. The molecular mechanism of the anti-proliferative activity of RKTS-33 and ECH has yet to be determined. RKTS-33 did not induce apoptosis in short-term culture in various tumor cell lines and showed weaker toxic activity than ECH in long-term culture. Therefore RKTS-33 might be a useful bioprobe that specifically blocks the FasL-dependent CTL-mediated killing pathway.

Acknowledgments

We thank Dr. N. Shinohara for cells and Dr. J. Tschopp and Dr. T. Suda for reagents. This work was supported by a grant-in-aid for scientific research from the Ministry of Education, Culture, Sports, Science and Technology of Japan and a research grant from the Naito Foundation. M.Y. was partly supported by a Grant from the 21st Century COE Program of the Ministry of Education, Culture, Sports, Science and Technology.

References

1) Barry, M., and Bleackley, R. C., Cytotoxic T lymphocytes: all roads lead to death. *Nat. Rev. Immunol.*, **2**, 401–409 (2002).
2) Russell, J. H., and Ley, T. J., Lymphocyte-mediated cytotoxicity. *Annu. Rev. Immunol.*, **20**, 323–370 (2002).
3) Metkar, S. S., Wang, B., Aguilar-Santelises, M., Raja, S. M., Uhlin-Hansen, L., Podack, E., Trapani, J. A., and Froelich, C. J., Cytotoxic cell granule-mediated apoptosis: perforin delivers granzyme B-serglycin complexes into target cells without plasma membrane pore formation. *Immunity*, **16**, 417–428 (2002).
4) Trapani, J. A., and Sutton, V. R., Granzyme B: pro-apoptotic, antiviral and antitumor functions. *Curr. Opin. Immunol.*, **15**, 533–543 (2003).
5) Lieberman, J., and Fan, Z., Nuclear war: the granzyme A-bomb. *Curr. Opin. Immunol.*, **15**, 553–559 (2003).
6) Nagata, S., Apoptosis by death factor. *Cell*, **88**, 355–365 (1997).
7) Krammer, P. H., CD95's deadly mission in the immune system. *Nature*, **407**, 789–795 (2000).
8) Miyake, Y., Kakeya, H., Kataoka, T., and Osada, H., Epoxycyclohexenone inhibits Fas-mediated apoptosis by blocking activation of pro-caspase-8 in the death-inducing signaling complex. *J. Biol. Chem.*, **278**, 11213–11220 (2003).
9) Mitsui, T., Miyake, Y., Kakeya, H., Osada, H., and Kataoka, T., ECH, an epoxycyclohexenone derivative that specifically inhibits Fas ligand-dependent apoptosis in CTL-mediated cytotoxicity. *J. Immunol.*, **172**, 3428–3436 (2004).
10) Kakeya, H., Miyake, Y., Shoji, M., Kishida, S., Hayashi, Y., Kataoka, T., and Osada, H., Novel non-peptide inhibitors targeting death receptor-mediated apoptosis. *Bioorg. Med. Chem. Lett.*, **13**, 3743–3746 (2003).
11) Staerz, U. D., Kanagawa, O., and Bevan, M. J., Hybrid antibodies can target sites for attack by T cells. *Nature*, **314**, 628–631 (1985).
12) Shinohara, N., Huang, Y. Y., and Muroyama, A., Specific suppression of antibody responses by soluble protein-specific, class II-restricted cytolytic T lymphocyte clones. *Eur. J. Immunol.*, **21**, 23–27 (1991).
13) Hanabuchi, S., Koyanagi, M., Kawasaki, A., Shinohara, N., Matsuzawa, A., Nishimura, Y., Kobayashi, Y., Yonehara, S., Yagita, H., and Okumura, K., Fas and its ligand in a general mechanism of T-cell-mediated cytotoxicity. *Proc. Natl. Acad. Sci. U.S.A.*, **91**, 4930–4934 (1994).
14) Watanabe, M., Wegmann, D. R., Ochi, A., and Hozumi, N., Antigen presentation by a B-cell line transfected with cloned immunoglobulin heavy- and light-chain genes specific for a defined hapten. *Proc. Natl. Acad. Sci. U.S.A.*, **83**, 5247–5251 (1986).
15) Kataoka, T., Shinohara, N., Takayama, H., Takaku, K., Kondo, S., Yonehara, S., and Nagai, K., Concanamycin A, a powerful tool for characterization and estimation of contribution of perforin- and Fas-based lytic pathways in cell-mediated cytotoxicity. *J. Immunol.*, **156**, 3678–3686 (1996).
16) Schneider, P., Holler, N., Bodmer, J. L., Hahne, M., Frei, K., Fontana, A., and Tschopp, J., Conversion of membrane-bound Fas(CD95) ligand to its soluble form is associated with downregulation of its proapoptotic activity and loss of liver toxicity. *J. Exp. Med.*, **187**, 1205–1213 (1998).
17) Miwa, K., Hashimoto, H., Yatomi, T., Nakamura, N., Nagata, S., and Suda, T., Therapeutic effect of an anti-Fas ligand mAb on lethal graft-versus-host disease. *Int. Immunol.*, **11**, 925–931 (1999).
18) Takayama, H., Shinohara, N., Kawasaki, A., Someya, Y., Hanaoka, S., Kojima, H., Yagita, H., Okumura, K., and Shinkai, Y., Antigen-specific directional target cell lysis by perforin-negative T lymphocyte clones. *Int. Immunol.*, **3**, 1149–1156 (1991).
19) Tanaka, M., Suda, T., Haze, K., Nakamura, N., Sato, K., Kimura, F., Motoyoshi, K., Mizuki, M., Tagawa, S., Ohga, S., Hatake, K., Drummond, A. H., and Nagata, S., Fas ligand in human serum. *Nat. Med.*, **2**, 317–322 (1996).

Epoxytwinol A, a novel unique angiogenesis inhibitor with C_2 symmetry, produced by a fungus†

Hideaki Kakeya,*[a] Rie Onose,[a] Hiroyuki Koshino[b] and Hiroyuki Osada*[a]

Received (in Cambridge, UK) 27th January 2005, Accepted 3rd March 2005
First published as an Advance Article on the web 15th March 2005
DOI: 10.1039/b501392e

We isolated a novel unique pentaketide dimer designated as epoxytwinol A from the fermentation broth of a fungus. The structure of epoxytwinol A was determined to have a new carbon skeleton with C_2 symmetry by elucidation of spectroscopic evidence. Epoxytwinol A inhibited endothelial cell migration stimulated by vascular endothelial growth factor (ED_{100} = 2.6 μM).

Vascular endothelial growth factor (VEGF) plays a central regulatory role as one of the most potent pro-angiogenic factors.[1] It regulates differentiation, migration, proliferation, capillary tube formation, and survival of endothelial cells. Thus, novel small molecules that control the VEGF-induced signal transduction pathway in endothelial cells hold great promise both as bioprobes (a biochemical tool) in the field of angiogenesis, and in drug development related to antiangiogenic therapy.[2] In our attempts to discover new inhibitors of angiogenesis from microbial metabolites,[3] we have isolated and carried out structure determination of epoxyquinols A (**1**) and B (**2**) (Fig. 1), novel unique pentaketide dimers produced by an uncharacterized fungus isolated from a soil sample.[4,5] During our continuous search for the same fungal metabolites, we have discovered a novel natural product

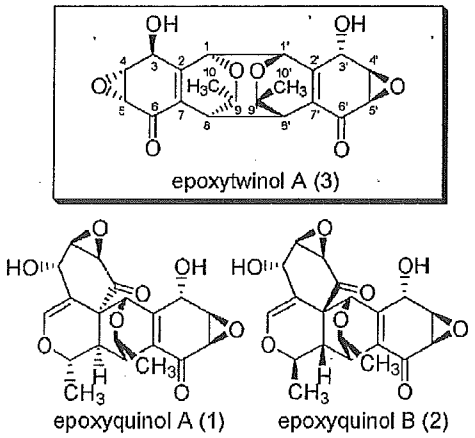

Fig. 1 Structures of epoxyquinols A (**1**) and B (**2**), and epoxytwinol A (**3**).

† Abbreviations used: DEPT, distortionless enhancement by polarization transfer; PFG, pulse field gradient; COSY, correlated spectroscopy; DQF, double quantum filtered; HMQC, heteronuclear multiple quantum coherence; HMBC, heteronuclear multiple-bond correlation; NOE, nuclear Overhauser effect.

*hkakeya@riken.jp (Hideaki Kakeya)
hisyo@riken.jp (Hiroyuki Osada)

designated as epoxytwinol A (**3**) that has a novel unique 17,19-dioxapentacyclo[8.6.2.$2^{2,9}$.$0^{3,8}$.$0^{11,16}$]icosa-3(8),11(16)-diene skeleton with C_2 symmetry.[6] We describe herein the isolation, spectroscopic structural elucidation, and biological properties of **3**.

The producing fungal strain was cultivated in a 30-litre jar fermenter containing 18 litres of fermentation medium for 4 days at 28 °C. The broth filtrate, adjusted to pH 7.0, was extracted with the same volume of ethyl acetate. The organic extract, concentrated *in vacuo*, was applied to a silica gel column and chromatographed using 0–50% methanol in chloroform in a stepwise manner. Epoxytwinol A (**3**) was eluted with 2% methanol in chloroform, and further separated by reversed-phase HPLC. Finally, purification by thin layer chromatography, using $CHCl_3$–MeOH = 30:1 as a solvent, afforded 9 mg of **3** as colorless oil. The molecular formula of **3** was established as $C_{20}H_{20}O_8$ on the basis of high-resolution EI-MS (found: *m/z* 388.1173, calcd: *m/z* 388.1158). UV spectra showed absorption maxima (ε) at 238 (7490) and 255 (sh, 6590) nm in methanol. The IR spectra showed characteristic bands at 3450, 1670, 1620, and 1255 cm^{-1}, indicating the presence of hydroxyl and α,β-unsaturated ketone carbonyl groups.

The ^{13}C NMR spectrum of **3** in acetone-d_6 shows 10 signals, indicating the presence of a proper axis of symmetry, not a plane or point symmetry, since the compound is optically active, $[\alpha]_D^{21}$ +303.3 (*c* 0.184, in acetone). The ^{13}C NMR and DEPT spectra revealed the presence of oxygen-bearing sp^3 methine carbons (δ 53.46, 58.46, 66.20, 72.83, and 81.57), an sp^3 methine carbon (δ 39.93), sp^2 quaternary carbons (δ 132.69 and 155.59), a carbonyl carbon (δ 192.66), and a methyl carbon (δ 23.01). In the ^1H NMR spectrum measured in acetone-d_6, eight signals were observed. An exchangeable proton was observed in the downfield region at 4.36 ppm due to the presence of hydroxyl groups that were quenched by the addition of D_2O. A methyl group at 0.76 ppm (d, 6.3) was observed together with oxygenated methine protons at 3.52 (dd, 3.4, 1.0), 3.85 (dd, 3.4, 1.0), 4.19 (q, 6.3), 4.60 (br d, 9.1), and 4.79 (s) ppm as well as a methine proton at 3.21 (s) ppm. The PFG-HMQC spectrum revealed all of the one-bond ^1H–^{13}C connectivities (Table 1). The PFG-DQF-COSY spectrum confirmed the presence of two partial structures (Fig. 2-a): (i) two epoxy methine and adjacent hydroxyl methine carbons and (ii) two sequential methine protons with a terminal methyl group. The connectivities of those partial structures and the remaining sp^3 methine carbon (δ 81.57) and quaternary carbons were determined by analysis of ^1H–^{13}C long-range correlations of the PFG-HMBC spectrum (Fig. 2-b). The important long-range correlations are as follows. From the epoxy methine H-5 at 3.52 ppm and a methine proton H-8 at 3.21 ppm (β to the C-10 methyl group) to α,β-unsaturated carbonyl carbon C-6 (δ 192.66) and sp^2

Table 1 ^{13}C (150 MHz) and ^{1}H (600 MHz) NMR data for epoxytwinol A (3) in acetone-d_6

Number	^{13}C (multiplicity)	$^{1}J_{CH}$ (Hz)[a]	^{1}H (multiplicity)	J (Hz)
1, 1′	81.57 (d)	152.9	4.79 (s)	
2, 2′	155.59 (s)			
3, 3′	66.20 (d)	145.0	4.60 (br d)	9.1
4, 4′	58.46 (d)	181.5	3.85 (dd)	3.4, 1.0
5, 5′	53.46 (d)	187.5	3.52 (dd)	3.4, 1.0
6, 6′	192.66 (s)			
7, 7′	132.69 (s)			
8, 8′	39.93 (d)	136.3	3.21 (s)	
9, 9′	72.83 (d)	148.8	4.19 (q)	6.3
10, 10′	23.01 (q)	129.0	0.76 (d)	6.3
3-OH, 3′-OH			4.36 (br d)	9.1

[a] $^{1}J_{CH}$ values were determined by the PFG-HMQC non-decoupling method.

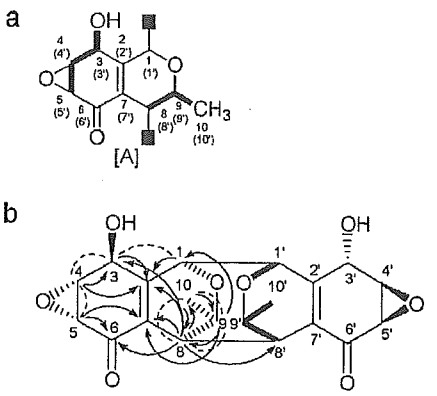

Fig. 2 (a) Partial structure [A] of epoxytwinol A (3). (Bold lines show significant proton spin networks in the PFG-DQF-COSY spectrum.) (b) PFG-HMBC and NOE data summary for epoxytwinol A (3). Data show half of the whole parts. (Arrows show ^{1}H–^{13}C long-range correlations in the PFG-HMBC spectrum, and dotted lines indicate significant NOEs.)

quaternary carbon C-7 (δ 132.69). The sp^2 carbon C-2 (δ 155.59) (β to the C-6 ketone group) has long-range correlations from H-1, H-3, H-4, and H-8 methine protons. Long-range correlations are also observed from an oxygenated methine H-9 at 4.19 ppm to C-7 and two methine carbons C-1 (δ 81.57) and C-8 (δ 39.93).

Thus, the corresponding monomer structure [A] was established as shown in Fig. 2-a. The molecular formula of 3 indicates that the index of hydrogen deficiency is 11, 5 of which account for the monomer structure [A]. Because the structure of 3 is dimeric, 10 unsaturations can be attributed to 2 units of the structure [A], leaving 1 unassigned unsaturation and indicating that epoxytwinol A (3) is pentacyclic. Of a few "dimeric" structures that can account for the structural features outlined above, only one, the structure of 3, exhibits optical activity. The connectivities of C-1 and C-1′ and of C-8 and C-8′ are confirmed by the 2D non-decoupling PFG-HMQC spectrum. In this spectrum, COSY cross-peaks between H-1 and H-1′, and between H-8 and H-8′ are observed with *cis* large vicinal coupling constant values of 8.8 and 12.2 Hz, respectively. $^{2}J_{H,C}$ values between H-8 and C-8′ of 5.4 Hz are obtained from the spectrum. In the HMBC spectrum, the lack of correlation between H-1 and C-1′ is caused by the $^{2}J_{H,C}$ value of almost 0 Hz, which is confirmed by the 2D non-decoupling PFG-HMQC spectrum. The small coupling constant values of $^{3}J_{H\text{-}3,H\text{-}4}$ ($^{3}J_{H\text{-}3',H\text{-}4}$) confirm that the relative stereochemistry between hydroxyl and epoxy groups has a *trans* configuration.[4,7] Significant coupling between H-8 and H-9 in the ^{1}H NMR spectrum was not observed, indicating that the dihedral angle between H-8 and H-9 would be *ca.* 90°. Furthermore, NOE differential spectra of 3 established the relative stereochemistry (Fig. 2-b). In particular, a large NOE enhancement between H-8 and H-10, as well as between H-1 and H-3, confirmed the stereochemistry. Thus, based on these NMR data and the physicochemical properties, the relative stereochemistry of 3 was unambiguously determined to be as shown in Fig. 1.

Epoxytwinol A (3) is composed of the same part that has been fused together *via* intermolecular [4+4] cycloaddition of the predicted 2*H*-pyran monomer compound 5 (Scheme 1). The precursor 5 would be generated from compound 4, which was also isolated from the same fungal metabolites. Epoxyquinols A (1) and B (2) could be formed *via* an *endo*/*exo* Diels–Alder reaction of 5 and/or its diastereomer at the C-9 methyl group,[4,5] which is supported by the biomimetic asymmetric total synthesis of 1 and 2 *via* the oxidative dimerization of 4.[8] There have been several reports of the intermolecular/intramolecular photo-[4+4] cycloaddition of 2-pyridone mixtures[9] or 2-pyridones with 1,3-dienes.[10] However, the reports of natural products similar to 3 with C_2 symmetry in microbial metabolites is rare. Furthermore, the synthetic methodology for [4+4] cycloaddition of polyketide compounds with 1,3-dienes has not been studied in detail. Very recently, asymmetric total synthesis of 3 has been completed, with the absolute configuration of 3 having been determined as shown in Fig. 1.[11] The mechanisms of intermolecular [4+4] cycloaddition of 2*H*-pyran monomer 5 and their derivatives are now being experimentally and theoretically investigated.

Epoxytwinol A (3) inhibits the human endothelial cell (HUVEC) migration induced by VEGF in a dose-dependent

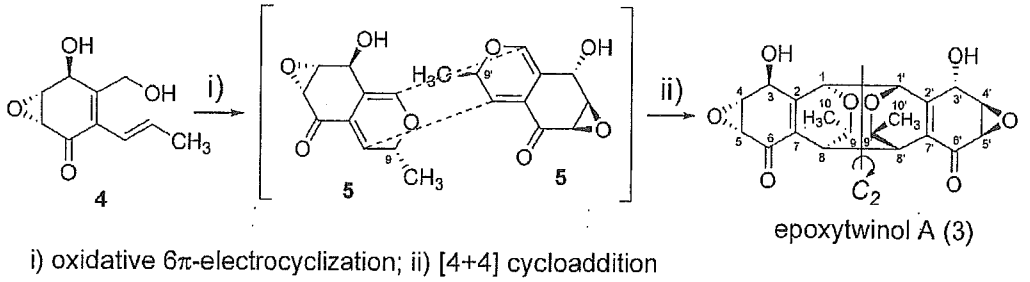

i) oxidative 6π-electrocyclization; ii) [4+4] cycloaddition

Scheme 1 Possible biosynthetic pathway of epoxytwinol A (3).

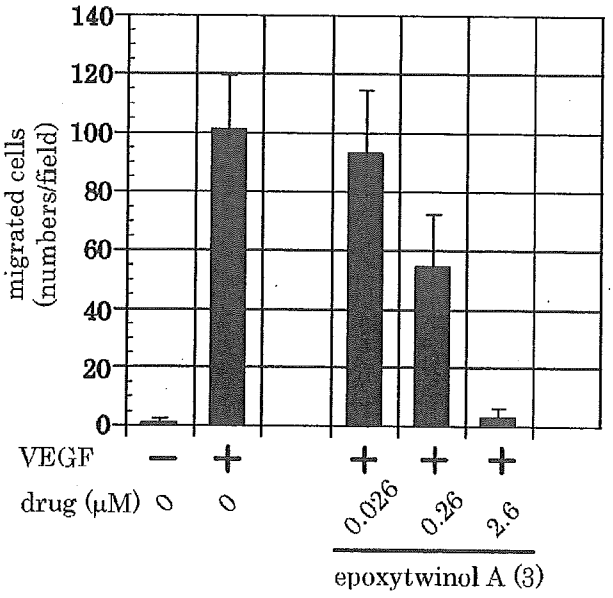

Fig. 3 Inhibitory activity by epoxytwinol A (**3**) on VEGF-induced cell migration in HUVECs.

manner, as shown in Fig. 3.[12] The ED_{100} value of **3** at 2.6 μM is more potent than that of **1** and the same as that of **2** (ED_{100} of **1** = 7.7 μM).[4,5] These results suggest that both the monomer core [A] and its bridge frame would be useful for the drug design of this series of novel angiogenesis inhibitors.

Further chemical and biological studies as well as studies of the biosynthetic pathways of **3** are now underway.

This work was supported in part by a Grant-in-Aid from the Ministry of Education, Culture, Sports, Science, and Technology of Japan, by a Grant-in-Aid for Cancer Research from the Ministry of Health, Labour, and Welfare of Japan, and by Special Project Funding for Basic Science (Chemical Biology Project) from RIKEN.

Hideaki Kakeya,*[a] Rie Onose,[a] Hiroyuki Koshino[b] and Hiroyuki Osada*[a]
[a]*Antibiotics Laboratory, Discovery Research Institute, RIKEN, 2-1 Hirosawa, Wako, Saitama 351-0198, Japan. E-mail: hkakeya@riken.jp; hisyo@riken.jp; Fax: +81 48 467 9542; Tel: +81 48 462 4669*
[b]*AD&SC, RIKEN, 2-1 Hirosawa, Wako, Saitama 351-0198, Japan*

Notes and references

1 J. Folkman, *Nat. Med.*, 1995, **1**, 27; D. Hanahan and J. Folkman, *Cell*, 1996, **86**, 353; W. Riasu, *Nature*, 1997, **386**, 671; M. Shibuya, *Cell Struct. Funct.*, 2001, **26**, 25; M. Shibuya, *Cancer Sci.*, 2003, **94**, 751.
2 N. Ferrara and K. Alitalo, *Nat. Med.*, 1999, **5**, 1359; D. Gasparini, *Drugs*, 1998, **58**, 17.
3 Y. Asami, H. Kakeya, R. Onose, A. Yoshida, H. Matsuzaki and H. Osada, *Org. Lett.*, 2002, **4**, 2845; H.-R. Ko, H. Kakeya, A. Arika, R. Onose, M. Ueki, M. Muroi, A. Takatsuki, H. Matsuzaki and H. Osada, *J. Microbiol. Biotechnol.*, 2002, **12**, 829; Y. Asami, H. Kakeya, R. Onose, Y.-H. Chang, M. Toi and H. Osada, *Tetrahedron*, 2004, **60**, 7085.
4 H. Kakeya, R. Onose, H. Koshino, A. Yoshida, K. Kobayashi, S.-I. Kageyama and H. Osada, *J. Am. Chem. Soc.*, 2002, **124**, 3496.
5 H. Kakeya, R. Onose, A. Yoshida, H. Koshino and H. Osada, *J. Antibiot.*, 2002, **55**, 829.
6 H. Osada, H. Kakeya, H. Konno and S. Kanazawa, *PCT Int. Appl.*, 2002, WO0288137. We named RKB-3564D in the PCT as epoxytwinol A (**3**).
7 T. Fex and B. Wickberg, *Acta Chem. Scand. Ser. B*, 1981, **35**, 97; R. L. Edwards, D. J. Maitland, I. J. Scowen, A. J. T. De Sousa and A. J. S. Whalley, *J. Chem. Soc., Perkin Trans 1*, 2001, 537.
8 M. Shoji, J. Yamaguchi, H. Kakeya, H. Osada and Y. Hayashi, *Angew. Chem. Int. Ed.*, 2002, **41**, 3192; C. Li, S. Bardhan, E. A. Pace, M.-C. Liang, T. D. Gilmore and J. A. Porco, Jr., *Org. Lett.*, 2002, **4**, 3267; G. Mehta and K. Islam, *Tetrahedron Lett.*, 2004, **45**, 3611; S. Kuwahara and S. Imada, *Tetrahedron Lett.*, 2005, **46**, 547.
9 E. C. Taylor and W. W. Paudler, *Tetrahedron Lett.*, 1960, **25**, 1; S. M. Sieburth, C.-H. Lin and D. Rucando, *J. Org. Chem.*, 1999, **64**, 950.
10 E. Sato, Y. Ikeda and Y. Kanaoka, *Liebigs Ann. Chem.*, 1989, 781.
11 M. Shoji, H. Imai, M. Mukaida, K. Sakai, H. Kakeya, H. Osada and Y. Hayashi, *J. Org. Chem.*, 2005, **70**, 79; C. Li and J. A. Porco, Jr., *J. Am. Chem. Soc.*, 2004, **126**, 1310.
12 VEGF-induced migration assay protocol: human umbilical vein endothelial cells (HUVEC) (1×10^5) suspended in HuMedia-EG2 medium (KURABO, Osaka) with various concentrations of **3**, were added to the upper compartment of a CHEMOTAXICELL chamber (KURABO, Osaka) and incubated with HuMedia-EG2 medium containing 12.5 ng ml^{-1} of VEGF in the lower compartment for 18 hours at 37 °C in a 5% CO_2 atmosphere. The filter was fixed with MeOH and stained with hematoxylin. The cells on the upper surface of the filter were removed by wiping with cotton swabs. Cells that migrated through the filter to the areas of the lower surface were counted manually under a microscope at a magnification of ×100. Values are means ± SD for triplicate samples.

JOC Article

Enantio- and Diastereoselective Total Synthesis of EI-1941−1, −2, and −3, Inhibitors of Interleukin-1β Converting Enzyme, and Biological Properties of Their Derivatives

Mitsuru Shoji,[†] Takao Uno,[†] Hideaki Kakeya,[‡] Rie Onose,[‡] Isamu Shiina,[§] Hiroyuki Osada,[‡] and Yujiro Hayashi*,[†]

Department of Industrial Chemistry, Faculty of Engineering, and Department of Applied Chemistry, Faculty of Science, Tokyo University of Science, Kagurazaka, Shinjuku-ku, Tokyo 162-8601, Japan, and Antibiotics Laboratory, Discovery Research Institute, RIKEN, 2-1 Hirosawa, Wako, Saitama 351-0198, Japan

hayashi@ci.kagu.tus.ac.jp

Received August 5, 2005

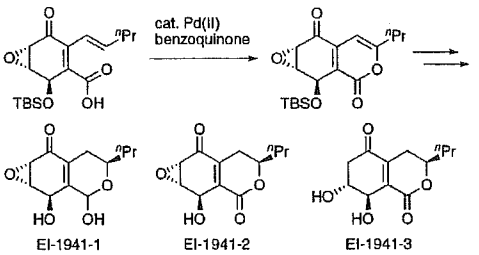

The first asymmetric total synthesis of EI-1941−1, −2, and −3, inhibitors of the interleukin-1β converting enzyme (ICE), has been accomplished, starting from a chiral epoxy iodoquinone **11**, a key intermediate in our total synthesis of epoxyquinols A and B. Despite a failure to synthesize the inhibitors by our postulated biosynthetic route, we were able to diastereoselectively synthesize them via an intramolecular carboxypalladation with the key steps being a 6-endo cyclization mode followed by β-hydride elimination. The investigation of the biological properties of EI-1941−1, −2, and −3 and their derivatives disclosed them to be potent and effective ICE inhibitors with less cytotoxicity than EI-1941−1 and −2 in a cultured cell system.

Introduction

Interleukin-1β (IL-1β) is an important mediator of pathogenesis of rheumatoid arthritis, septic shock, inflammation, and other physiological conditions.[1] IL-1β converting enzyme (ICE) is a cysteine protease, which cleaves a biologically inactive 31 kDa precursor to biologically active IL-1β.[2] IL-1β is released from macrophage-like cells in an inflammatory situation, and is the major form of IL-1 in diseases. ICE inhibitors have been shown to prevent inflammation in several acute models,[3] suggesting that ICE inhibitors would be useful as antiinflammatory drugs. Recently, Koizumi and coworkers have isolated EI-1941−1 (**1**), EI-1941−2 (**2**), and EI-1941−3 (**3**) from culture broths of *Farrowia* sp., the first two of which selectively inhibit human recombinant ICE activity with IC_{50} values of 0.086 and 0.006 μM, respectively, whereas the last is inactive at concentrations up to 10 μM in an in vitro system.[4] EI-1941−2 also has weak antimicrobial activities against Gram-positive

* Phone: +81 3-5228-8318. Fax: +81 3-5261-4631.
[†] Department of Industrial Chemistry, Faculty of Engineering, Tokyo University of Science.
[§] Department of Applied Chemistry, Faculty of Science, Tokyo University of Science.
[‡] RIKEN.

(1) (a) Dinarello, C. A. *Blood* **1991**, *77*, 1627. (b) Dinarello, C. A.; Wolff, S. M. *N. Engl. J. Med.* **1993**, *328*, 106.

(2) (a) Thornberry, N. A.; Bull, H. G.; Calaycay, J. R.; Chapman, K. T.; Howard, A. D.; Kostura, M. J.; Miller, D. K.; Molineaux, S. M.; Weidner, J. R.; Aunins, J.; Elliston, K. O.; Ayala, J. M.; Casano, F. J.; Chin, J.; Ding, G. J.-F.; Egger, L. A.; Gaffney, E. P.; Limjuco, G.; Palyha, O. C.; Raju, S. M.; Roland, A. M.; Salley, J. P.; Yamin, T.-T.; Lee, J. A.; Shively, J. E.; Maccross, M.; Mumford, R. A.; Schmidt, J. A.; Tocci, M. J. *Nature* **1992**, *356*, 768. (b) Gerretti, D. P.; Kozlosky, C. J.; Mosley, B.; Nelson, N.; Ness, K. V.; Greenstreet, T. A.; March, C. J.; Kronheim, S. R.; Druck, T.; Cannizzaro, L. A.; Huebner, K.; Black, R. A. *Science* **1992**, *256*, 97.

(3) Ku, G.; Faust, T.; Lauffer, L. L.; Livingston, D. J.; Harding, M. W. *Cytokine* **1996**, *8*, 377.

(4) (a) Koizumi, F.; Matsuda, Y.; Nakanishi, S. *J. Antibiot.* **2003**, *56*, 464. (b) Koizumi, F.; Ishiguro, H.; Ando, K.; Kondo, H.; Yoshida, M.; Matsuda, Y.; Nakanishi, S. *J. Antibiot.* **2003**, *56*, 603.

10.1021/jo0516436 CCC: $30.25
Published on Web 11/03/2005